Dalton Transactions

Cite this: *Dalton Trans.*, 2011, **40**, 5865

www.rsc.org/dalton

PAPER

Metastable Se_6 as a ligand for Ag^+: from isolated molecular to polymeric 1D and 2D structures†‡

Damian Aris,[a] Johannes Beck,[b] Andreas Decken,[a] Isabelle Dionne,[a] Jörn Schmedt auf der Günne,*[c] Wilfried Hoffbauer,[b] Tobias Köchner,[d] Ingo Krossing,*[d] Jack Passmore,*[a] Eric Rivard,[a] Folker Steden[b] and Xinping Wang[a]

Received 17th September 2010, Accepted 11th March 2011
DOI: 10.1039/c0dt01251c

Attempts to prepare the hitherto unknown Se_6^{2+} cation by the reaction of elemental selenium and Ag[A] ([A]$^-$ = $[Sb(OTeF_5)_6]^-$, $[Al(OC(CF_3)_3)_4]^-$) in SO_2 led to the formation of $[(OSO)Ag(Se_6)Ag(OSO)][Sb(OTeF_5)_6]_2$ **1** and $[(OSO)_2Ag(Se_6)Ag(OSO)_2][Al(OC(CF_3)_3)_4]_2$ **2a**. **1** could only be prepared by using bromine as co-oxidant, however, bulk **2b** (**2a** with loss of SO_2) was accessible from $Ag[Al(OC(CF_3)_3)_4]$ and grey Se in SO_2 (chem. analysis). The reactions of $Ag[MF_6]$ (M = As, Sb) and elemental selenium led to crystals of $1/\infty\{[Ag(Se_6)]_\infty[Ag_2(SbF_6)_3]_\infty\}$ **3** and $\{1/\infty[Ag(Se_6)Ag]_\infty\}[AsF_6]_2$ **4**. Pure bulk **4** was best prepared by the reaction of $Se_4[AsF_6]_2$, silver metal and elemental selenium. Attempts to prepare bulk **1** and **3** were unsuccessful. **1–4** were characterized by single-crystal X-ray structure determinations, **2b** and **4** additionally by chemical analysis and **4** also by X-ray powder diffraction, FT-Raman and FT-IR spectroscopy. Application of the PRESTO III sequence allowed for the first time ^{109}Ag MAS NMR investigations of **4** as well as AgF, AgF_2, $AgMF_6$ and $\{1/\infty[Ag(I_2)]_\infty\}[MF_6]$ (M = As, Sb). Compounds **1** and **2a/b**, with the very large counter ions, contain isolated $[Ag(Se_6)Ag]^{2+}$ heterocubane units consisting of a Se_6 molecule bicapped by two silver cations (local D_{3d} sym). **3** and **4**, with the smaller anions, contain close packed stacked arrays of Se_6 rings with Ag^+ residing in octahedral holes. Each Ag^+ ion coordinates to three selenium atoms of each adjacent Se_6 ring. **4** contains $[Ag(Se_6)^+]_\infty$ stacks additionally linked by $Ag(2)^+$ into a two dimensional network. **3** features a remarkable 3-dimensional $[Ag_2(SbF_6)_3]^-$ anion held together by strong Sb–F···Ag contacts between the component Ag^+ and $[SbF_6]^-$ ions. The hexagonal channels formed by the $[Ag_2(SbF_6)_3]^-$ anions are filled by stacks of $[Ag(Se_6)^+]_\infty$ cations. Overall **1–4** are new members of the rare class of metal complexes of neutral main group elemental clusters, in which the main group element is positively polarized due to coordination to a metal ion. Notably, **1** to **4** include the commonly metastable Se_6 molecule as a ligand. The structure, bonding and thermodynamics of **1** to **4** were investigated with the help of quantum chemical calculations (PBE0/TZVPP and (RI-)MP2/TZVPP, in part including COSMO solvation) and Born–Fajans–Haber-cycle calculations. From an analysis of all the available data it appears that the formation of the usually metastable Se_6 molecule from grey selenium is thermodynamically driven by the coordination to the Ag^+ ions.

Introduction

Numerous molecular cyclic sulfur and selenium allotropes E_n (E = S: n = 6–15, 18, 20 *etc.*; E = Se: n = 6, 7, 8) that are isolable at r.t. have been prepared and structurally characterized. Molecular S_8 is the most stable form of sulfur and the stability of the selenium allotropes increases in the order: $Se_7 < Se_6 < Se_8 < Se_\infty$.[1–5] Metastable chair-$Se_6$ was inserted into mordenite, Zeolite Y and a SiO_2 matrix.[6–8] Hexagonal Te_∞ is the only stable allotrope of tellurium. Salts of the isolated molecular diamagnetic

[a]*Department of Chemistry, University of New Brunswick, Fredericton N.B., E3B 6E2, Canada. E-mail: passmore@unb.ca; Fax: +1 (506) 453-4981*
[b]*Institut für Anorganische Chemie, Friedrich Wilhelms Universität Bonn, 53121, Bonn, Germany*
[c]*Department Chemie, Ludwig Maximilians Universität, 81377, München, Germany*
[d]*Institut für Anorganische und Analytische Chemie, Albert-Ludwigs-Universität, 79104, Freiburg, Germany*

† Jörn Schmedt auf der Günne (^{109}Ag/^{19}F NMR), Ingo Krossing (theoretical calculations and isolated $[(OSO)_xAgSe_6Ag(OSO)_x]^{2+}$ (x = 1, 2) preparation), and Jack Passmore (problem conception and the remainder of preparations and structures).

‡ Electronic supplementary information (ESI) available: see text for details. CCDC reference number 814799; CSD reference numbers 418699–418701. For ESI and crystallographic data in CIF or other electronic format see DOI: 10.1039/c0dt01251c

homopolyatomic cations S_n^{2+} (n = 4, 8, 19), Se_n^{2+} (n = 4, 8, 10, 17) and Te_n^{m+}(n = 4, 6, 7, 10, m = 2; n = 8, m = 2, 4) contain positively charged rings formed upon oxidation of the elements with non basic anions.[9–17] Few examples where a partial positive charge is induced onto an electronegative main group element cluster on coordination to a metal ion like Ag^+ are known, and require that the counterion is weakly basic like $[MF_6]^-$ (M = As, Sb), $[Sb(OTeF_5)_6]^-$ or the $[Al(OR_F)_4]^-$ aluminates (R_F = $C(CF_3)_3$, $C(H)(CF_3)_2$): *e.g.* $[Ag(S_8)_n]^+$,[18,19] $[Ag(P_4)_n]^+$[20–22] (n = 1, 2), $[Ag(I_2)^+]_\infty$[23] and $[Ag(P_4S_3)_n]^+$[24,25] (n = 1–3). One of us prepared and characterized the cations $[Se_6I^+]_\infty$ and $[Se_6I_2]^{2+}$,[26,27] which can be viewed as containing Se_6 coordinated to "I^+". Other related selenium cations include $[Se_7Se_2Cl]^+$[28] and $[Ph_2Se_6]^{2+}$.[29] There are also some examples of hexaselenium, heptaselenium and nonaselenium coordinated to a transition metal ($PdCl_2(Se_6)$,[30] $PdBr_2(Se_6)$,[30] $(AgI)_2Se_6$,[31] $Re_2I_2(CO)(Se_7)$[32,33] and $Rh_2Se_9Cl_6$[34]). Salts containing cationic stacks of $[Rb(Se_8)^+]_\infty$[35] and $[Rb(Se_6)_2^+]_\infty$,[36] in which a weak interaction between Rb^+ and the selenium rings was postulated, are known. Crown-shaped Te_8 rings were stabilized in Cs_3Te_{22} in the coordination sphere of the caesium atom, which is surrounded by a cube of tellurium atoms from two Te_8 rings.[37] $AgTe_3[AsF_6]$ has been reported but no structural characterization was presented.[38]

Herein we report on reactions of grey selenium and Ag[A] ([A]$^-$ = $[Sb(OTeF_5)_6]^-$,[39–41] $[Al(OC(CF_3)_3)_4]^-$, $[AsF_6]^-$ and $[SbF_6]^-$) forming $[(OSO)Ag(Se_6)Ag(OSO)][Sb(OTeF_5)_6]_2$ **1**, $[(OSO)_2Ag(Se_6)Ag(OSO)_2][Al(OC(CF_3)_3)_4]_2$ **2a**, $1/\infty\{[Ag(Se_6)]_\infty[Ag_2(SbF_6)_3]_\infty\}$ **3** and $\{1/\infty[Ag_2(Se_6)]_\infty\}[AsF_6]_2$ **4**. Each of these salts contains partially oxidised metastable hexaselenium rings in a chair conformation coordinated to Ag^+. The crystal structures of **1**, **3** and **4** were already published in 2004 in a short communication.[42]

Results and discussion

Synthesis of single crystal 1 and attempts to prepare bulk 1

Attempts to prepare $Se_6[Sb(OTeF_5)_6]_2$ containing the hitherto unknown Se_6^{2+} dication (*cf.* Te_6^{2+})[12] by the reaction of elemental selenium and $Ag[Sb(OTeF_5)_6]$ in SO_2 (molar ratio 3–7 Se : 1 Ag^+) led to $Se_{10}[Sb(OTeF_5)_6]_2$ as the only identifiable selenium product (^{77}Se-NMR). The oxidation power of the reactants was increased by the addition of bromine with the hope that the reaction would proceed according to eqn (1).

$$6\ Se + Br_2 \rightarrow \{Br_2Se_6\} \xrightarrow{2Ag[Sb(OTeF_5)_6]} Se_6[Sb(OTeF_5)_6]_2 + 2\ AgBr \quad (1)$$

The reaction gave yellow needle-like crystals, which were unsuitable for X-ray diffraction studies, and from which Raman and ^{77}Se NMR spectra could not be obtained. However, storage of an oily reaction product for three months at ambient temperature yielded large yellow-orange cubes of **1** (X-ray structure). We were unable to prepare **1** directly from selenium and $Ag[Sb(OTeF_5)_6]$, but always observed the formation of Se cations in SO_2 solution by ^{77}Se-NMR spectroscopy (Se_{10}^{2+}, and upon cooling to –70 °C also small amounts of Se_8^{2+}).

Syntheses of 2a/b, 3, and 4

A direct synthesis of the closely related compound **2a** became possible with the use of $Ag[Al(OC(CF_3)_3)_4]$ and grey selenium powder in SO_2 (eqn (2)).

$$2\ Ag[Al(OC(CF_3)_3)_4] + 6\ Se_{grey} + 4\ SO_2 \xrightarrow{\text{Ultra Sound (U.S.) 6 h}} [(OSO)Ag(Se_6)Ag(OSO)][Al(OC(CF_3)_3)_4]_2 \quad (2)$$

During the reaction the greyish suspension turned increasingly green (maximum at two hours) then later became brown-orange. This observation is related to the reaction leading to **1**: the ^{77}Se-NMR spectra of which indicated the intermediate formation of brown Se_{10}^{2+} as well as small amounts of (green) Se_8^{2+}. Attempts to directly detect these Se-dications in reactions leading to **2a** by solution ^{77}Se-NMR spectroscopy were unsuccessful due to the exceedingly low concentrations of the intermediate species. The observed signals of NMR reactions with the suitable stoichiometry to give **2a** at δ^{77}Se = 1074.4, 982.3 and 862.3 in a saturated SO_2 solution of **2a** could neither be assigned to free Se_6, Se_7, Se_8 rings nor to selenium cations (Se_4^{2+}, Se_8^{2+}, Se_{10}^{2+}). The spectra are characterised by a poor signal to noise ratio even after 27000 scans at 298 and 233 K (delay 5 s, acquisition time 0.84 s; original spectra deposited in the ESI‡). This may be attributed to underlying dynamic exchange processes, which is supported by DFT-calculations including COSMO solvation (see below).

Orange needle shaped crystals of **2a** were obtained reproducibly by cooling the crude oily product to 2 °C (yield 67% crystalline material). Attempts to obtain Raman spectra of **2a** failed even at 100 K and with low laser energy due to fluorescence and sample decomposition in the Laser beam. Samples of **2b** gave X-ray powder patterns of microcrystalline materials with large cell parameters that are different to those simulated with the cell parameters of **2a** (S10‡). An elemental analysis of crystals of the same batch had only minor sulfur content (exp. 0.17%), but otherwise was in agreement with the formulation of a salt $[Ag_2(Se_6)(SO_2)_x][Al(OC(CF_3)_3)_4]_2$ with x being < 0.1. Thus, upon isolation of **2b**, probably the weakly bound SO_2 in **2a** is almost completely lost.

Small amounts of single crystals of **3** and **4** were obtained by the reactions of a large excess of $Ag[SbF_6]$ and $Ag[AsF_6]$ with selenium powder with short reaction time in liquid SO_2, followed by filtration and formation of crystals of **3** and **4** after a few minutes. It is possible that $[Ag_x(Se_6)(SO_2)_y]^{x+}$ intermediates (x = 1 and 2; y = 0–4) are present in a concentrated SO_2 solution of $Ag[MF_6]$, leading to the insoluble $[MF_6]^-$ salts of the polymeric $[Ag(Se_6)^+]$ cations (see calculations below).

Attempts to prepare bulk 3

Several reactions of various stoichiometries with selenium in both powder as well as pellet form and $Ag[SbF_6]$ were carried out (ESI S1.1 and S1.2‡) in attempts to prepare pure **3** in bulk quantities. The powder diffraction patterns of the resulting insoluble products do not clearly fit or contain the calculated pattern based on the single X-ray crystal structure of **3**; the nature of the insoluble products is not clear at this time. Their Raman spectra are similar, and show similar Se–Se and Se–Ag–Se stretching frequencies (ESI S1.3/S1.5‡). The reaction of $Ag[SbF_6]$ with excess Se pellets gave a solid with a chemical analysis consistent with the

formulation $Ag(Se_6)[SbF_6]$. In a large excess of $Ag[SbF_6]$, solid **3** was isolated from the solution (see above). It is likely that **3** is thermodynamically unstable in the presence of liquid sulfur dioxide with respect to the insoluble $\{1/\infty[Ag_2(Se_6)]_\infty\}[SbF_6]_2$, the $[SbF_6]^-$ analogue of **4**, and very soluble $Ag[SbF_6]$ (eqn (3)). Further loss of soluble $Ag[SbF_6]$ could also be envisaged (eqn (4)).

$$\frac{1}{n}\{[Ag(Se_6)][Ag_2(SbF_6)_3]\}_n \xrightarrow{SO_2} \frac{1}{n}\{[Ag_2(Se_6)][SbF_6]_2\}_n(s) + Ag[SbF_6] \quad (3)$$

$$\frac{1}{n}\{[Ag_2(Se_6)][SbF_6]_2\}_n(s) \xrightarrow{SO_2} \frac{1}{n}\{[Ag(Se_6)][SbF_6]\}_n + n\ Ag[SbF_6] \quad (4)$$

The ^{109}Ag solid state NMR confirmed the complexity of the $Se/Ag[SbF_6]$ reactions (ESI S1.7†).

Synthesis of bulk 4

Bulk **4** was prepared by the reaction of excess $Ag[AsF_6]$ and Se pellets (eqn (5)). Unreacted Se pellets were manually separated from the yellow insoluble product, from which a good quality Raman spectrum (ESI†), a ^{109}Ag-MAS-NMR (–42, –220 ppm) (Fig. 6), and a ^{19}F MAS-NMR spectrum (see Table 3) were obtained. The empirical formula of the insoluble product based both on weight changes and on chemical analysis, is in good accordance with that established from the single crystal structure determination of **4**. The reaction of $Ag[AsF_6]$ and excess Se pellets led to an insoluble product of a similar formulation. However, its Raman spectrum (ESI S1.3/S1.5‡) gave an additional peak (156 cm^{-1}), which might arise from an impurity or from a different phase of similar composition.

$$2\ Ag[AsF_6] + 6\ Se \xrightarrow{SO_2} \frac{1}{n}\{[Ag_2(Se_6)][AsF_6]_2\}_n \quad (5)$$

An alternative route to bulk **4** was provided by the reaction of $Se_4[AsF_6]_2$, silver metal and elemental selenium at room temperature (eqn (6)).

$$2\ Ag + 2\ Se + Se_4[AsF_6]_2 \xrightarrow{SO_2} \frac{1}{n}\{[Ag_2(Se_6)][AsF_6]_2\}_n \quad (6)$$

The Raman and IR spectra of the yellow insoluble product were identical to those from the reaction of excess $Ag[AsF_6]$ with Se pellets (ESI S1.3/S1.5‡). The X-ray powder diffraction patterns of the yellow insoluble product obtained by the two routes were identical and very similar to that calculated from the single crystal structure of **4** (ESI S1.8‡).

Crystal structures

All crystal structures **1–4** (Table 1, Fig. 1 and ESI S2‡) feature the remarkable, ideally D_{3d}-symmetric, $[Ag_2Se_6]$-heterocubane unit, derived from a Se_6 ring in chair conformation which is bicapped by two silver atoms.

The bond distances and angles of the Se_6 rings are quite similar to that in elemental Se_6 (see Table 1). The structure[26] of $[Se_6I_2]^{2+}$ can be considered as a less symmetric relative, in which symmetrically coordinating Ag^+ is substituted by asymmetrically interacting I^+ (see ESI S2.1.3†). The heterocubane $[Ag_2Se_6]^{2+}$ structure is related to that of the Nb_2Sn_6 moiety in $[Nb_2Sn_6(C_6H_5Me)_2]^{2-}$[43] (S2.1.2‡).

Structures containing isolated $[Ag_2(Se_6)]$ heterocubane units

Each silver atom in **1** is coordinated to one SO_2 molecule, which is threefold disordered maintaining the local D_{3d} symmetry (see ESI S2.1‡). **1** and **2a** contain discrete $[(OSO)Ag(Se_6)Ag(OSO)]^{2+}$ and $[(OSO)_2Ag(Se_6)Ag(OSO)_2]^{2+}$ dications and $[Sb(OTeF_5)_6]^-$ and $[Al(OC(CF_3)_3)_4]^-$ counter ions which have typical structures and (resolved) disorder inherent to these ions. See ESI for a comparison of anion bond distances and angles, and drawings of the disorder. The packing of ions is in agreement with the radius ratio rules (see ESI S2.1‡). The weak cation anion contacts (distances and valency units[44,45] (v.u.) given in Table 1), imply positive charge on all atoms in the $[Ag_2Se_6]^{2+}$ heterocubane in **1** and **2a**. The $Ag^+ \ldots OSO$ distance and v.u. in **1** (2.28(3) Å) is very similar to that in $OSO \ldots Ag[Al(OC(CF_3)_3)_4]$ (ESI S2.1.7‡), which was shown to be almost completely an ionic interaction as was the interaction in gaseous $Ag^+(OSO)_n$ ($n = 1, 2$).[46] The two $OSO \ldots Ag^+$ distances in **2a** are similar to **1** (Table 1) and also highly ionic. Thus, both **1** and **2a** contain discrete $[Ag_2Se_6]^{2+}$ heterocubane dications. One threefold disordered SO_2 per Ag in **1** leads to a $[Ag_2Se_6]^{2+}$ structure with local D_{3d} symmetry. **2a** contains two SO_2 per Ag^+ as well as a secondary contact to the silver atom of the adjacent cation (see Fig. 2) leading to an overall C_i-symmetry of $[Ag_2Se_6]^{2+}$ in **2a**. Additional weak $Ag^+ \ldots F$ contacts in **1** and **2a** lead to an (5 + 2) Ag^+ coordination, as is common in more ionic Ag^+ complexes[47] (ESI S2.1/S2.2‡).

Structures containing polymeric $[Ag(Se_6)^+]_\infty$ stacks

3 is constructed from a 1D $[Ag(Se_6)^+]_\infty$ cationic coordination polymer encapsulated by a honeycomb-like array of $[Ag_2(SbF_6)_3]^-$ anions (Fig. 1 and 3).

To the first order of approximation, the $[Ag(Se_6)^+]_\infty$ cation can be viewed as a stack of closed packed Se_6 rings with Ag^+ residing in the octahedral holes (see also ESI S2.3). Some related stacks can be found in the literature, *e.g.* $[Rb(Se_8)^+]_\infty$[35] (see ESI S2.3.7a) or $[Cs(Te_8)^+]_\infty$.[37] There are weak $F \ldots Se$ contacts as well as one fluorine $F \ldots Ag^+$ contact (Table 1) at 3.095(9) Å, which slightly distorts the ideal D_{3d} symmetry of the $[Ag_2Se_6]^{2+}$ fragment in the stack (see Fig. 1) and increases the coordination number of Ag^+ to seven. A detailed description of the $[Ag_2(SbF_6)_3]^-$ anion is given in the ESI (S2.3). It forms hexagonal channels that include the 1D $[Ag(Se_6)^+]_\infty$ stacks. Six silver atoms, that are bridged by six $[SbF_6]^-$ units, reside at each corner of the hexagonal cavity.

4 consists of similar $[Ag(Se_6)^+]_\infty$ stacks down the c-axis, cross linked by silver (Ag2) ions into infinite two dimensional networks in the ac-plane separated by $[AsF_6]^-$ anions (see Fig. 1 and 4). The two cross linking Ag–Se bond lengths are shorter (2.688(2) Å) than those in the stack (2.941(3), 2.927(2) Å; 6 per Se_6).

The cross-linked $[Ag(Se_6)^+]_\infty$ chains are related to those of $PdX_2(Se_6)$ (X = Cl, Br)[30] in which Se_6 is η^1-coordinated to Pd forming infinite chains. Normally chalcogen rings coordinate above the ring or in a lateral fashion,[32,33] but here both coordination modes are realised in a 2D structure for which only one related example $[Rh_2(O_2CCF_3)_4]_3(S_8)_2$ is found in the literature.[48] In **4** no silver fluorine contacts are found to the Ag^+ in the $[Ag(Se_6)^+]_\infty$ stack, but Ag2 is involved into multiple fluorine contacts, two from each of the four adjacent anions (Ag2-F1 2.689(6) (× 4), Ag2-F2 3.053(6) (× 4) Å).

Table 1 Selected structural parameters of crystal structures **1**, **2a**, **3** and **4**, calculated structures **A–C** (PBE0/TZVPP) and elemental Se_6. Bond valences[45] in italics. (number of occurrences is given by (value ×)). Sum of van der Waals radii (Ag . . . F = 3.2 Å, Ag . . . O = 3.2 Å, Se . . . F = 3.4 Å)

	1	**2a**	**3**	**4**	**A**[a]	**B**[a]	**C**[a]	Se_6 (s)[49]
d(Se–Se)/Å	2.346(2)	2.339(3) 2.353(3) 2.368(3)	2.345(2) 2.346(2)	2.339(3) 2.362(2)	2.356	2.325 2.353 2.393	2.326 2.354 2.392	2.356(3)
Se–Se(ave., Å)	2.346(2)	2.353(3)	2.346 (2)	2.354 (3)	2.356	2.357	2.357	2.356(3)
>(Se–Se–Se)/°	100.91(7)	100.16(10) 100.55(10) 99.75(10)	99.61(7) 99.68(6) 100.05(6)	98.48(7) 99.76(9)	101.54	99.44 99.62 100.67	99.16 100.73 102.91	101.1(1)
> Se–Se–Se(ave/°)	100.91(7)	100.15(10)	99.78(2)	98.91(5)	101.54	99.91	100.93	101.1(1)
> Se–Se–Se–Se(ave/°)	76.49(1)	77.64(10)	78.11(1)	79.78(3)	75.52	76.1	76.01	76.2(3)
d(Ag1–Se)/Å, *s*[*v.u.*]	2.885(2), *0.185*(3 ×)	2.791(3), *0.235*(1 ×) 2.893(3), *0.179*(1 ×) 2.950(3), *0.153*(1 ×)	3.0239(17), *0.127*(2 ×) 3.0636(16), *0.114*(2 ×) 2.8408(13), *0.208*(2 ×)	2.9273(18), *0.165*(4 ×) 2.941(3), *0.158*(2 ×)	2.903	2.756 2.929(2 ×)	2.744(2 ×) 2.946(4 ×)	
d(Ag1–Se) (ave./Å)	2.885	2.878	2.976	2.932				
Σ s(Ag1–Se), *s*[*v.u.*]	*0.555*	*0.567*	*0.898*	*0.976*				
d(Ag2–Se)/Å], *s*[*v.u.*] (in **4**)				2.688(3), *0.314* (2 ×)		2.575	2.581	
Σ s(Ag2–Se), *s*[*v.u.*]				0.628				
d(Ag1–O)/Å, *s*[*v.u.*]	2.28(3), *0.310* (1 ×)	2.362(15), *0.247* (1 ×) 2.439(17), *0.199* (1 ×)						
Σ s(Ag1–O), *s*[*v.u.*]		*0.446*						
d(Ag1–O′)/Å, *s*[*v.u.*] (in **2**)		3.139(1), *0.030* (1 ×)						
d(Ag1–F)/Å, *s*[*v.u.*]	2.988(4), *0.040*(3 ×)	3.02(2), *0.021*(1 ×)	3.095(1), *0.03* (1 ×)					
d(Ag2–F)/Å, *s*[*v.u.*] (in **4**)				2.689(6), *0.090*(4 ×) 3.053(6), *0.034*(4 ×)				
d(Se–F)/Å (# of contacts)	3.170–3.384(18 ×)	3.026–3.495 (24 ×)	2.912–3.218 (12 ×)	3.080–3.350 (28 ×)				
Σ*s*(*Ag1–F*), *s*[*v.u.*]	*0.120* (1 ×)		*0.03*					
Σ*s*(*Ag2–F*), *s*[*v.u.*] (in **4**)				*0.496*				
Σ*s*(*Ag1–X*), *s*[*v.u.*]	*0.985*	*1.064*	*0.928*	*0.976*				
Σ*s*(*Ag2–X*), *s*[*v.u.*] (in **4**)				*1.124*				

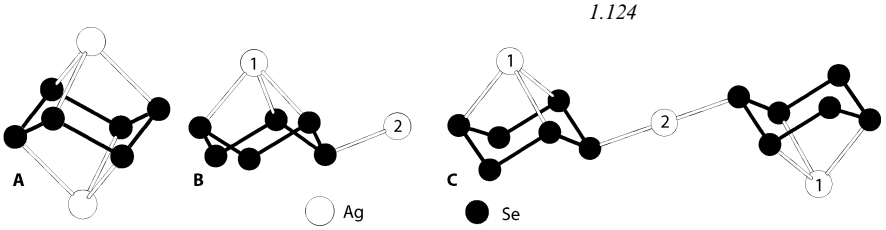

[a] See diagram.

All cations, regardless of whether they are more or less isolated as in **1** and **2a**, or if they are polymeric as in **3** and **4** bear numerous Se–F contacts ranging from 2.912 to 3.384 Å, indicating that positive charge is delocalized from the silver atoms to the selenium rings (see Table 1 below). All structural parameters of **1** to **4** as well as Se_6 and other related (in part calculated) compounds are compared in Table 1 below and more extensively in the ESI (see S2‡).

Quantum chemical calculations

To gain deeper insight into the structural features and bonding properties of these compounds various structures were calculated at different levels (See Table 1, Fig. 5, ESI‡). The key structural unit of compounds **1** to **4** is the D_{3d} symmetric $[Ag_2Se_6]^{2+}$ cation **A**, which is a building block to all structures discussed here. This unit was calculated at BP86/SVP, PBE0/TZVPP and (RI-)MP2/TZVPP levels to find an appropriate method for the structure calculation. Pure DFT with the rather small SVP basis set underestimates the Se–Se and Ag–Se distances significantly as this method intrinsically neglects dispersion. Hybrid DFT PBE0 with a larger triple ζ basis set leads to acceptable bonding parameters compared to the crystal structures. The Se–Se distances are slightly too long, but the Ag–Se distances are within the experimental error (longer distances in the crystal structures arise from coordination and deviation from the ideal D_{3d}-symmetry (*e.g.* crystal structure of **2a**). MP2 shows Se–Se distances which fit exactly the experimental values, but overestimated electron correlation leads to overly short Ag–Se distances. Thus, we decided to further investigate the system mainly using the PBE0/TZVPP method.

To prove the influence of further coordination to the silver atoms several other structures, inter alia $[(OSO)Ag(Se_6)Ag(OSO)]^{2+}$, $[(OSO)_2Ag(Se_6)Ag(OSO)_2]^{2+}$ and cationic fragments **B** and **C**—derived from crystal structures **3** and **4**—were optimised. The bond distances and angles of structures **A–C** (Table 1) are comparable to those found in the solid state and are therefore not discussed in detail. In contrast to this, the optimised structures **D** and **E** that were taken from the cation structures of **1** and **2a** show a significant deviation from the solid state arrangements (Fig. 5).

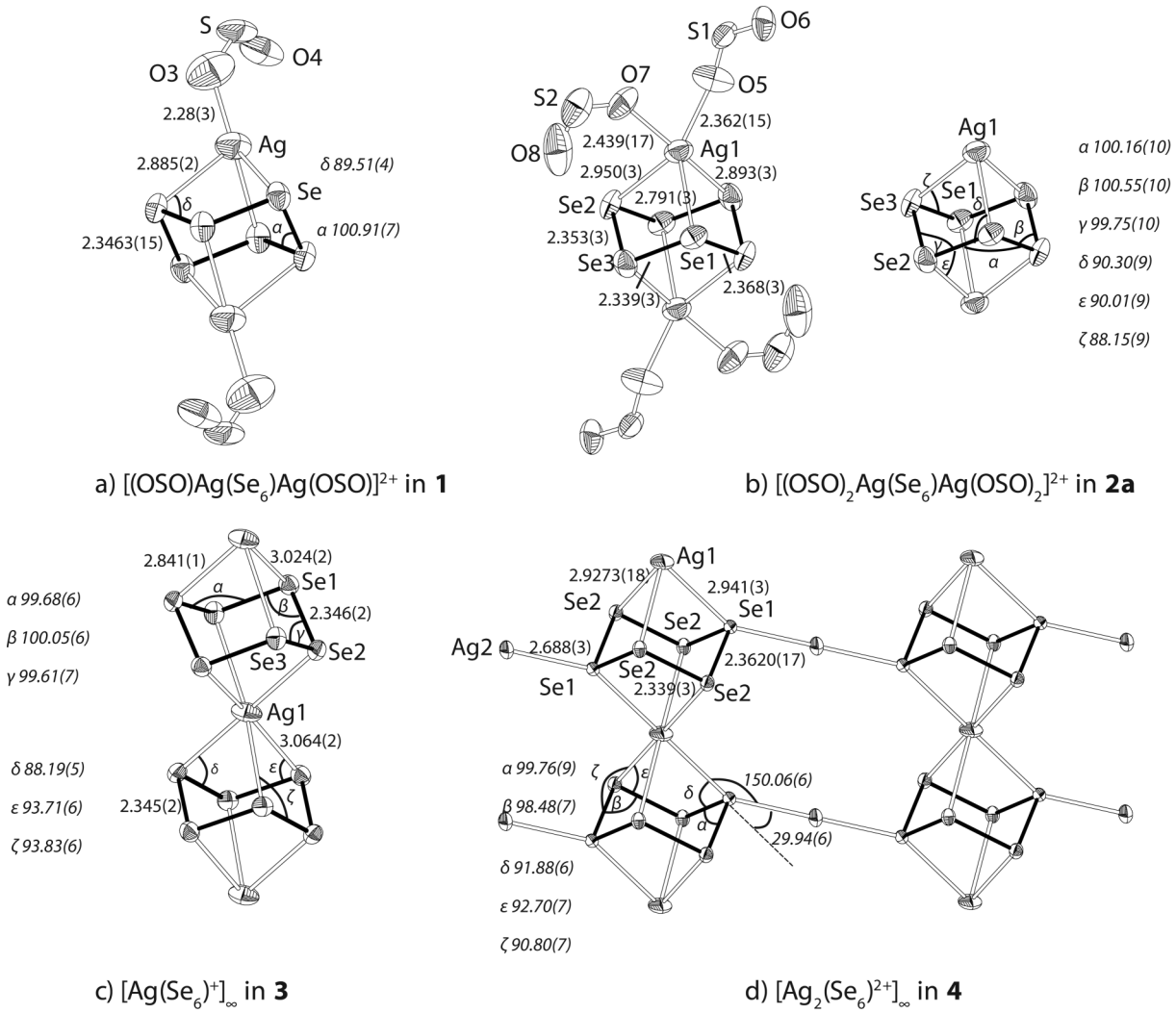

Fig. 1 Single crystal X-ray structures of cations in **1**, **2a**, **3** and **4**. Atomic distances in Å, and angles in degrees. The thermal ellipsoids are drawn at the 50% probability level.

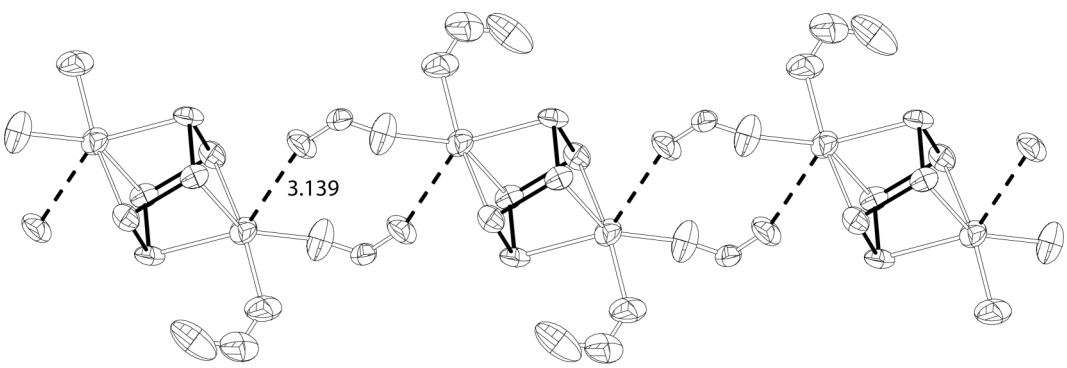

Fig. 2 Section of the cation stack in **2a** with Ag–O contacts (dashed lines/distance in Å). Thermal ellipsoids are shown with 50% probability.

The minimum geometry for $[(OSO)_2Ag(Se_6)Ag(OSO)_2]^{2+}$ **D** obtained by BP86/SVP leads to a structure that is significantly different from the solid state structure of **1** obtained *via* single crystal X-ray crystallography. Here only one η^1-silver–selenium bond is found (d = 2.532 Å), two other contacts (d = 3.845 Å) give a structure much closer to the C_{2h}-symmetric $[Se_6I_2]^{2+}$-unit. However, if the calculation is carried out with the more balanced PBE0/TZVPP hybrid HF-DFT-method, this effect on the bond lengths is attenuated. Three distances range from 2.782–3.045 Å, which are closer to, but still different from, the crystallographic

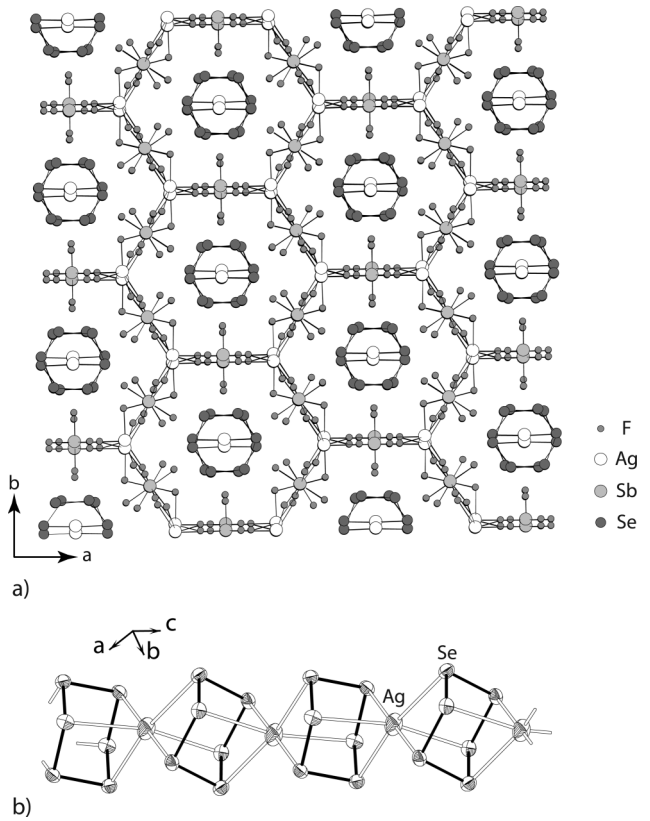

Fig. 3 a) A view of **3** down the c-axis; b) detail of one 1D polymeric $[Ag(Se_6)^+]_\infty$ strand of **3** along the c-axis.

values by up to 0.15 Å. MP2/TZVPP gives similar results with slightly shorter bond lengths. The Ag–(OSO) coordination in **D** reduces the symmetry of the central $[Ag_2Se_6]$-unit to C_i in the gas

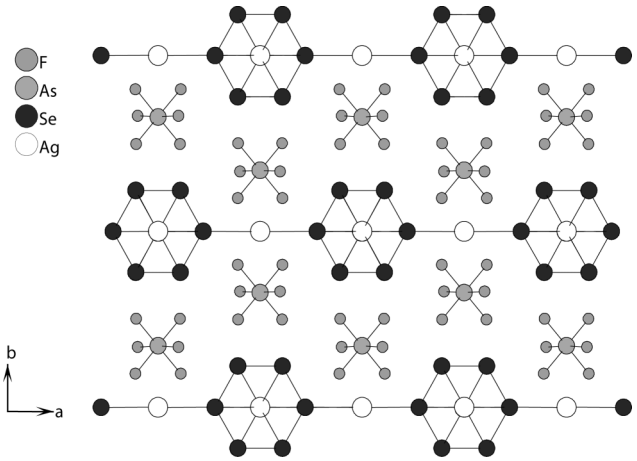

Fig. 4 A portion of **4** projected down the c-axis.

phase. Due to size restrictions, the calculation of the coordination of two additional SO_2 molecules in $[(OSO)_2Ag(Se_6)Ag(OSO)_2]^{2+}$ **E**[50] was only carried out at the PBE0/TZVPP level. When comparing the calculated structure of **E** to **2a**, one has to take into consideration that the experimental structure is a 1D coordination polymer and not an isolated structure (Fig. 2). In the gas phase one Ag–Se distance (3.295 Å) of **E** is rather long, which leads to the reduced η^2-silver-selenium coordination. Overall, the calculated gas phase structures of **D** and **E** show significant deviations from the crystal structures. Here the question emerged whether the structural features of dicationic **1** and **2a** were attainable by gas phase calculations in the absence of the solid state environment. Therefore, it appeared wise to include medium effects, as the lattice of an AB_2 salt may greatly influence the structure due to its inherent (but unknown) dielectric constant. A simple way to

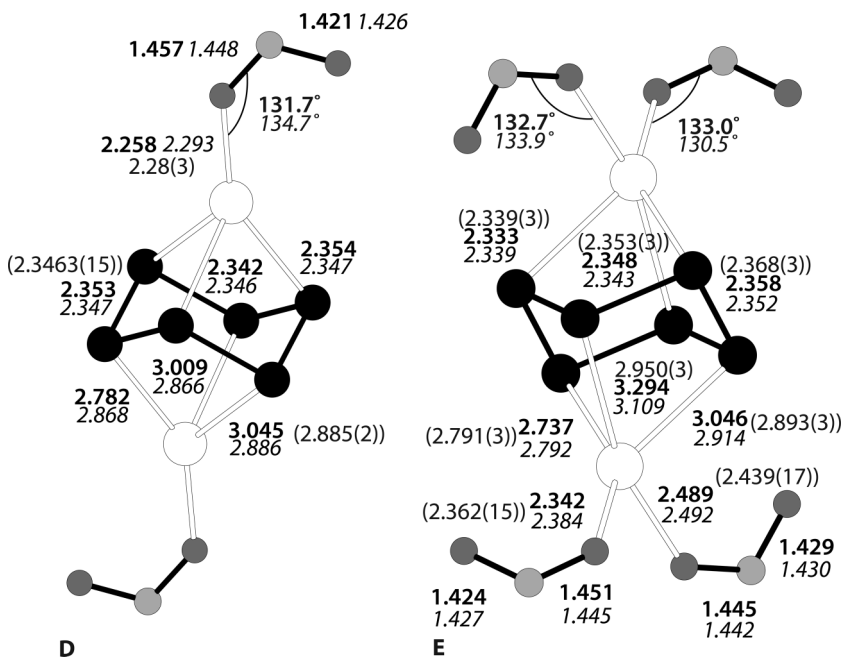

Fig. 5 Calculated structures **D** $[(OSO)Ag(Se_6)Ag(OSO)]^{2+}$ and **E** $[(OSO)_2Ag(Se_6)Ag(OSO)_2]^{2+}$. Values: in **bold** gas phase structures (PBE0/TZVPP); in *italics* structures optimised including COSMO solvation PBE0/TZVPP (COSMO; $\varepsilon_r = 16.3$); bond length in Å, angles in degrees. Experimental distances of the cations of structures **1** and **2a** are given in parentheses.

Table 2 Vibrational frequencies (cm^{-1}) for solid Se_6,[a] Se_6 in SiO_2 matrix,[b] $\{1/\infty[Se_6I]_\infty\}AsF_6$,[c] $PdCl_2(Se_6)$[d], **4**, $[AsF_6]^-$ (in $O_2[AsF_6]$)[e] (relative peak intensities in parentheses) and the calculated[f] fragments **A**, **B** and **C**[g]

				4		AsF_6^- (in O_2AsF_6)		A calc.[j]		B calc[j]	C calc[j]		
Solid Se_6 Raman	Se_6 in SiO_2 matrix	$\{1/\infty[Se_6I]_\infty\}[AsF_6^-]$[h] Raman	$PdCl_2Se_6$ Raman	Raman	IR	Raman	IR	Raman	IR	Vibration	Raman	IR	Assignments[i]
				712(1)	698 (10)		700(10)					713	$\nu_3(AsF_6^-)$, F_u
				691(1)									
		678(0.2)		673(5)	666(8)	689(10)		676		676	676		$\nu_1(AsF_6^-)$, A_g
		577(0.02)		574(0.5)		573(5)		*575*		575	575		$\nu_2(AsF_6^-)$, E_g
		571(0.02)											
		563(0.02)		558(0.5)	561(3)								
				401(0.5)	398(1)		385(1)		402	402		402	$\nu_4(AsF_6^-)$, F_u
					385(2)			360		360	360		
		364(0.05)		373(3)		375(1)							$\nu_5(AsF_6^-)$, F_g
				296(3)									ν (PdCl)
247(10)	276 (9)	275(2)	275(4)	272(10)				270, 268	268	284	284		ν(SeSe), A_{1g}
221(1)	263 (2)	256(1)	256(0.5)	256(5)						281, 263	281,	236	ν(SeSe), E_g
											262		
		234(10)	237(10)							267, 244	266,		ν(SeSe), E_u
											244		
										219	219		
		172(6)	201(0.3)	171(9)				**162**		**188**	**182**,	169	ν_s(SeAg2Se)
											166		
									178	172	119		ν_s(SeISe, SePdSe, SeAgSe)
129(3)	133 (2)	120(1)	125(4)	126(6)				110		125			δ(SeSeSe), A_{1g}
										117	**110**		**δ(SeAg1Se)**
										110			
102(2)	102(10)	113(3)	104(1)	113(5)					102		86		δ(SeSeSe), E_g
		104(2)											δ(SeI)
									97	89	88		ν_s(SeAg1Se)

[a] See reference [54]. [b] A microporous pure SiO_2 modification consisting of pseudohexagonal sheets of pentagondodecahedral cages, stacked in an ABCABC sequence and interconnected by O–Si–O bridges. See reference [8]. [c] I. Dionne, PhD thesis, University of New Brunswick, **2002**. For preparation, see reference [26,27]. [d] See reference [30]. [e] C. Naulin and R. Bougon, *J. Chem. Phys.*, **1976**, *64*, 4156. [f] Calculated frequencies below 85 cm^{-1} are not shown (see electronic supplementary information: Raman). [g] Peak intensities were determined by estimating the area (for Raman) and height (for IR) of peaks. [h] There is some combination of the SeSe stretching bands: 512 (intensity: 0.01, origin: 275 + 234), 491 (0.01, 256 + 234), 467 (0.01, 234 × 2), 442 (0.06, 275 + 172). [i] The AsF_6^- assignments are based on ideal O_h symmetry and for Se_6 on ideal D_{3d} symmetry. The actual symmetry in O_2AsF_6 in **4** is O_h, however C_2 in **4**, and C_i in $(Se_6I)_n{\cdot}nAsF_6$, thus leading to additional bands. [j] Fragment A, (D_{3d}), Fragment B (C_1), no selection rules, Fragment C (C_{2h}). Idealized symmetries which may differ from real solid state. Additional or less bands may occur in the synthesized compounds.

include medium effects and to overcome the Coulomb repulsion between the two silver ions in the gas phase is to employ the COSMO solvation model. Both **D** and **E** were optimised at the PBE0/TZVPP level with the COSMO[51] model (ε_r = 16.3 (SO_2 298 K[52]). When these medium effects are included, the $[Ag_2Se_6]^{2+}$-unit in **D** turns almost D_{3d} symmetric (d_{AgSe} = 2.866, 2.868, 2.886 Å) within 0.02 Å from the crystal structure **1**. In **E** one longer bond at 3.109 Å and two shorter bonds at 2.792 and 2.914 Å give an asymmetric η^3-coordination to the Ag^+ ion. Overall it appears that the inclusion of medium effects leads to a better agreement between the experimental and calculated structures.

Vibrational spectra of 4

The Raman spectrum (ESI S4‡) shows the bands attributable to the polymeric $[Ag_2(Se_6)^{2+}]_\infty$ cation and that of an isolated $[AsF_6]^-$ anion. The bands at 272, 256, 126 and 113 cm^{-1} are assigned to Se_6 ring vibrations (Table 2). The symmetric Se–Se stretches (272 and 256 cm^{-1}) are at higher frequencies than those found in solid Se_6 (247 and 221 cm^{-1}),[53,54] indicative of stronger Se–Se bonds in $[Ag(Se_6)^+]_\infty$ than found in solid Se_6, which possesses a large number of significant intermolecular $Se_6 \cdots Se_6$ contacts

Table 3 Summary of the ^{109}Ag and ^{19}F chemical shifts and ^1J coupling constants in the solid state

Compound	δ_{iso} (^{109}Ag)	δ_{iso} (^{19}F)	$^1J(^{19}F, X)$/Hz[a]
AgF	–47[b]	–318.2	—
AgF_2	–189	–199.5	—
$Ag[SbF_6]$	–221	–127.7	unresolved
$Ag[AsF_6]$	–243	–67.6,	975, 975
$\{1/\infty[Ag(I_2)]_\infty\}[SbF_6]$	119	–75.4	2077
$\{1/\infty[Ag(I_2)]_\infty\}[AsF_6]$	112	–110.6	977
$\{1/\infty[Ag_2(Se_6)]_\infty\}[AsF_6]_2$, **4**	–42	–53.4	970
	–220	–56.5	

[a] X = As, Sb. [b] Our measurement of the ^{109}Ag NMR of solid AgF (–47 ppm) gives a different result compared to that of a previous study of a static sample (–110 (15) ppm) probably owing to the higher resolution of our MAS experiment.[59]

reducing the effective Se–Se bonding within the ring, but similar to that observed for the Se_6 rings isolated in mordenite, Zeolite Y and SiO_2 matrix. The Se_6 Raman frequencies and intensities in $[Ag(Se_6)^+]_\infty$ are similar to those in $[Se_6I^+]_\infty$ and $PdCl_2(Se_6)$ (Fig. 9(c) and Table 3) except for an additional Se–Se stretch at 237 cm^{-1} in $PdCl_2(Se_6)$ (and $PdBr_2(Se_6)$) and 234 cm^{-1} in $\{1/\infty[Se_6I]_\infty\}[AsF_6]$.

This likely reflects the smaller Se–Se bond alternation and smaller variation of Se–Se bond lengths in $[Ag(Se_6)^+]_\infty$, compared to $PdCl_2(Se_6)$ and $[Se_6I^+]_\infty$.

The band observed at 171 cm^{-1} for **4** can be assigned to υ_s(SeAgSe), which is consistent with the symmetric stretching vibrational frequency for υ_s(SeISe) in $(Se_6I^+)_n$ (172 cm^{-1}) and υ_s(SePdSe) in $PdCl_2Se_6$ (201 cm^{-1}). A similar intense Raman band was also observed for υ_s (I–Ag–I) in $\{1/\infty[Ag(I_2)]_\infty\}[SbF_6]$[23] (99 cm^{-1}) and υ_s (N–Ag–N) in $Ag(NH_3)_2^+$ (211 cm^{-1}).[55] Whether this band (171 cm^{-1}) is due to the Se–Ag2–Se stretch or the Se–Ag1–Se stretch or an overlap of both was investigated by quantum mechanical calculations (PBE0/TZVPP)[56] of the Se–Ag–Se-framework models **A**, **B** and **C** shown below Table 1: Calculated spectra of fragments **B** and **C** in Table 2 show bands at 188 cm^{-1} (low calculated scattering activity) and 161 cm^{-1} that are mainly composed of a Se–Ag2–Se stretching vibration with small admixtures of Se–Ag1–Se. Nevertheless the isolated $[Ag_2Se_6]^{2+}$-model **A** also has a mode at 162 cm^{-1}, which consists of a combination of Se_6-stretching that also bears a significant amount of a Se–Ag1–Se vibration. However, the Raman-intense Se–Ag1–Se frequencies of **A** are calculated to occur significantly lower at around 100 cm^{-1}. Thus, the calculations of the model compounds suggest that the assignment of the experimental 171 cm^{-1} band is more likely a Se–Ag2–Se stretch.

$^{109}Ag\{^{19}F\}$ polarization transfer MAS NMR spectra of 4, $\{1/\infty[Ag(I_2)]_\infty\}[MF_6]$ (M = As, Sb) and related fluorine-containing compounds

The ^{109}Ag NMR spectra were obtained with the recently introduced pulse technique PRESTO,[57] which is much less demanding to the NMR probe than ordinary ^{109}Ag cross polarization magic angle spinning (CP-MAS) experiments. This allowed the determination of the ^{109}Ag chemical shift values of the crystalline compounds in a relatively short time and to overcome the relative low receptivity (28% of that for natural abundance ^{13}C) of ^{109}Ag.[58] AgF was the only silver-fluorine compound that was investigated prior to this work by static ^{109}Ag NMR experiments. Here we report the first examples (Table 3) of high-resolution ^{109}Ag signals by using PRESTO-III (from ^{19}F to ^{109}Ag). In each structure of $Ag[MF_6]$ and $\{1/\infty[Ag(I_2)]_\infty\}[MF_6]$ (M = As, Sb), there is only a single crystallographically independent Ag atom, consistent with a single peak in the recorded ^{109}Ag NMR spectra. Due to anisotropic chemical shifts rotation side bands are observed in the ^{109}Ag spectra of $\{1/\infty[Ag(I_2)]_\infty\}[MF_6]$ (M = As, Sb) (ESI S5.2.2,‡ for M = Sb). The ^{109}Ag chemical shift in solid $Ag[SbF_6]$ is –221 ppm, representing a deshielding of 22 ppm with respect to that of solid $Ag[AsF_6]$ (–243 ppm), which is consistent with different chemical environment of Ag as in $Ag[SbF_6]$, Ag is surrounded by six F atoms (the shortest Ag–F distance is 2.505(2) Å) while in $Ag[AsF_6]$, Ag is surrounded by ten F atoms (the shortest Ag–F distance is 2.220(5) Å). A similar, but smaller deshielding (7 ppm), was observed for $\{1/\infty[Ag(I_2)]_\infty\}[MF_6]$ relative to the Sb homologue. The ^{109}Ag MAS NMR spectrum of **4** has two peaks (Fig. 6). The resonance at –220 ppm could be assigned to Ag(2) that is similar to that of $Ag[SbF_6]$ and has some Ag–F interactions and the peak at –42 ppm to Ag(1) with no fluorine contacts.

Gas phase, solution and solid state thermodynamics of 1 and 2A

In order to understand the thermodynamics of the formation of the $[Ag_2Se_6]^{2+}$ cations several other species were calculated in addition to those shown above. Detailed information on their structure and energetics can be found in the ESI‡ (S4.1/S4.2). The gas phase enthalpies and the Gibbs energies were calculated at the PBE0/tzvpp level for the formation of possible reaction products. Gibbs free solvation energies, which have great influence on the thermochemistry, were taken into account using the conductor-like screening model COSMO with a dielectric constant of ε_r = 16.3[52] (SO_2, 298 K).[60] All results are summarized in Table 4.

The formation of $[Ag_2Se_6]^{2+}$ at 298.15 K in the gas phase is exothermic (Δ_rH = –120 kJ mol^{-1}) and becomes more favourable with the addition of two SO_2 molecules (Δ_rH = –298 kJ mol^{-1}) and about 100 kJ mol^{-1} more favourable still with addition of two further SO_2 molecules (less Coulomb repulsion by delocalisation of positive charge). Gibbs energies show the great influence of the loss of entropy for this reaction. The reaction of silver ions, selenium and SO_2 leading directly to $[(OSO)Ag(Se_6)Ag(OSO)]^{2+}$ and $[(OSO)_2Ag(Se_6)Ag(OSO)_2]^{2+}$ are exergonic with Δ_rG = –186 kJ mol^{-1} and –193 kJ mol^{-1} respectively. If solvation is taken into account the Gibbs energy remains exergonic with –185 kJ mol^{-1} **1**, and –125 mol^{-1} for **2a**. However, it is much more appropriate to use the $Ag(OSO)^+$ and $Ag(OSO)_2^+$ cations as models in solution. The comparison of the Gibbs energies shows that in solution the coordination of Se_6 to form $[Ag_2Se_6]^{2+}$ is in preference to Ag–SO_2 coordination (about 50 kJ mol^{-1}). In solution the coordination of two SO_2 molecules (**1**) to the $[Ag_2Se_6]^{2+}$ unit is favoured by Δ_rG = –37 kJ mol^{-1}; the coordination of four SO_2 endergonic

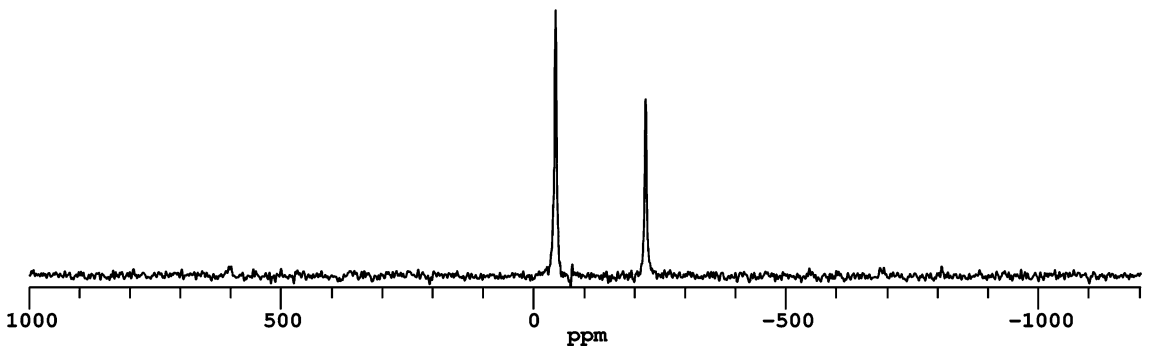

Fig. 6 $^{109}Ag\{^{19}F\}$ MAS NMR spectrum of **4** obtained with the PRESTO-III sequence.

Table 4 Calculated thermodynamics for formation and decomposition reactions of $[(OSO)Ag(Se_6)Ag(OSO)]^{2+}$ in **1**, $[(OSO)_2Ag(Se_6)Ag(OSO)_2]^{2+}$ in **2a**, $[Ag_2Se_6]^{2+}$, Se_6^{2+} and Se_8^{2+} in the gas phase and SO_2 solution at 298 K. Values in kJ mol^{-1} (PBE0/TZVPP)

Reaction	$\Delta_r H^0$	$\Delta_r G^0$	$\Delta_r G^0{}_{solv.}$
$2\ SO_2 + Ag^+ \rightarrow Ag(OSO)_2^+$	−196	−140	−49
$Ag(OSO)_2^+ + SO_2 \rightarrow Ag(OSO)_3^+$	−44	−23	−1
$Se_6 + 2\ Ag^+ \rightarrow [Ag_2Se_6]^{2+}$	−120	−57	−148
$[Ag_2Se_6]^{2+} + 2\ SO_2 \rightarrow [(OSO)Ag(Se_6)Ag(OSO)]^{2+}$ (in **1**)	−177	−129	−37
$[Ag_2Se_6]^{2+} + 4\ SO_2 \rightarrow [(OSO)_2Ag(Se_6)Ag(OSO)_2]^{2+}$ (in **2a**)	−276	−136	+23
$Se_6 + 2\ Ag^+ + 2\ SO_2 \rightarrow [(OSO)Ag(Se_6)Ag(OSO)]^{2+}$ (in **1**)	−298	−186	−185
$Se_6 + 2\ Ag^+ + 4\ SO_2 \rightarrow [(OSO)_2Ag(Se_6)Ag(OSO)_2]^{2+}$ (in **2a**)	−397	−193	−125
$Se_6 + 2\ Ag(OSO)^+ \rightarrow [(OSO)Ag(Se_6)Ag(OSO)]^{2+}$	−93	−32	−132
$Se_6 + 2\ Ag(OSO)_2^+ \rightarrow [(OSO)_2Ag(Se_6)Ag(OSO)_2]^{2+}$	−5	+86	−28
$2\ Ag(SO_2)_2^+ + [(OSO)_2Ag(Se_6)Ag(OSO)_2]^{2+} \rightarrow 2\ Ag(OSO)_3^+ + [(OSO)Ag(Se_6)Ag(OSO)]^{2+}$	+11	−39	−61
$[(OSO)_2Ag(Se_6)Ag(OSO)_2]^{2+} \rightarrow Ag(OSO)_2^+ + [(OSO)AgSe_6]^+$	−123	−182	−23
$[(OSO)Ag(Se_6)Ag(OSO)]^{2+} \rightarrow Ag(OSO)^+ + [(OSO)AgSe_6]^+$	−102	−132	+39
$[(OSO)Ag(Se_6)Ag(OSO)]^{2+} + SO_2 \rightarrow Ag(OSO)_2^+ + [(OSO)AgSe_6]^+$	−195	−195	+16
$[(OSO)Ag(Se_6)Ag(OSO)]^{2+} + 2\ SO_2 \rightarrow Ag(OSO)_2^+ + [(OSO)AgSe_6]^+$	−222	−189	+36
$Se_8 + 2\ Ag^+ \rightarrow Se_8^{2+} + 2\ Ag$	+418[a]	$\approx\Delta_r H^{0,b}$	+519
$Se_8 + 2\ Ag^+ \rightarrow Se_8^{2+} + Ag_2$	+248	+273	+182
$6\ Se_{grey(s)} + 2\ Ag(OSO)_2^+{}_{(solv)} \rightarrow Se_6^{2+}{}_{(boat,\ solv)} + 4\ SO_{2(solv)} + 2\ Ag^0{}_{(s)}$			+130
$6\ Se_{grey(s)} + 2\ Ag(OSO)_2^+{}_{(solv)} \rightarrow Se_6^{2+}{}_{(chair,\ solv)} + 4\ SO_{2(solv)} + 2\ Ag^0{}_{(s)}$			+147
$8\ Se_{grey(s)} + 2\ Ag(OSO)_2^+{}_{(solv)} \rightarrow Se_8^{2+}{}_{(solv)} + 4\ SO_{2(solv)} + 2\ Ag^0{}_{(s)}$			+122

[a] These reactions were calculated as follows: $\{Se_{6\ or\ 8} \rightarrow Se_{6\ or\ 8}^{2+} = \Sigma\ (1st\ IE + 2nd\ IE)\} + \{2\ Ag^+ \rightarrow 2\ Ag\ (-2 \times IE\ Ag)\}$. [b] Entropy contributions are approximately 0.

by +23 kJ mol^{-1}(**2a**). Nonetheless, complex **2a** is formed in the solid state, which is attributed to a gain in lattice enthalpy (see below).

The ^{77}Se NMR spectra of **2** at 298 and 233 K (three ^{77}Se unassigned resonances) suggest a dynamic system of coordination and dissociation of SO_2 and Se_6 to Ag^+, which may be accompanied by selenium cation formation. This picture is completely supported by the calculated Gibbs energies in SO_2 solution in Table 4. Nevertheless, the pivotal question remaining is, why the synthesis of Se_6^{2+} was unsuccessful, while Se_8^{2+} and Se_{10}^{2+} were at least visible in the NMR spectra as intermediates. Two possible isomers of a hypothetical Se_6^{2+} were calculated (ESI‡ S5.5) with a relative enthalpy difference of 24 kJ mol^{-1} in favour of the boat conformer (*cf.* the known boat Te_6^{2+}).[61,62] As expected, the oxidation $\Delta_r H$(g) and $\Delta_r G$(g) of Se_6 by two Ag^+ to form both isomers of Se_6^{2+} and elemental silver is highly unlikely in the gas phase. Also the oxidation of Se_8 to give the known[12] Se_8^{2+} dication is unfavourable in the gas phase. If solvation is considered the Gibbs reaction energy of the formation of the selenium cations remains endergonic. The description of open shell systems with COSMO is not advisable because it may be grossly misleading. Therefore the calculation was performed with the closed shell silver dimer. Nevertheless this system is purely hypothetical and far away from the true nature of the solvated system. At last a Born–Fajans–Haber-cycle starting from elemental selenium and solvated $Ag(OSO)_2^+$ leading to solvated selenium cations and solid silver metal gives a more reliable picture. The formation of the solvated cations is estimated to be endergonic by 122 kJ mol^{-1} (Se_8^{2+}) to 147 kJ mol^{-1} (Se_6^{2+} chair). Nonetheless the ^{77}Se-NMR-spectrum gave evidence for the formation of Se_8^{2+}. Therefore Se_6^{2+} might indeed also be formed and could be one of the three unassigned signals.

This leads to the question to what extent the solid state influences the thermodynamics. An estimation of the lattice potential energies using the empirically derived formula refined by Jenkins was carried out. For this Volume Based Approach the volume of the anions and cations were taken from the literature or otherwise were calculated with COSMO (Table deposited with ESI‡ S4.2.1). The reaction enthalpies leading to the solid products were assigned with Born–Fajans–Haber-cycles using the calculated gas phase enthalpies collected in Table 4 (Scheme 1). The sublimation enthalpy $\Delta_{sub}H$ from grey selenium leading to Se_6(g) is 138.6 kJ mol^{-1},[63] the lattice enthalpy $\Delta_{latt}H$ of $Ag[Sb(OTeF_5)_6]$ was calculated to be 366 kJ mol^{-1} and the value for $\Delta_{vap}H^{298\ K}(SO_2)$[52] is 23 kJ mol^{-1}. The lattice enthalpy of **1** was calculated as 1027 kJ mol^{-1} leading to the reaction enthalpy $\Delta_r H$ (s) in Scheme 1 of −415 kJ mol^{-1}. The results for different possible products are summarized in Table 5.

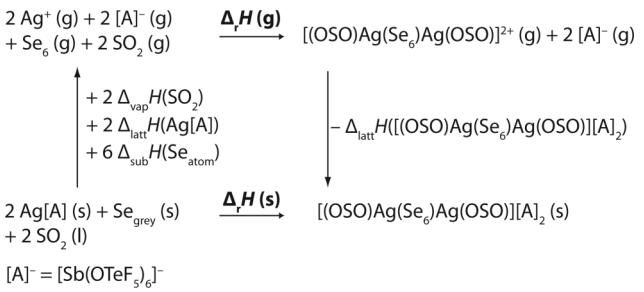

Scheme 1 Born–Fajans–Haber cycle for the estimation of the solid state thermodynamics of the formation of **1** from grey selenium, $Ag[Sb(OTeF_5)_6]$ and SO_2.

Using a related approach the solid state reaction enthalpies of several competing reactions were investigated (all cycles and auxiliary data are deposited in the ESI‡ S4.1 and S4.2). All results are collected in Table 5.

Since the $[Al(OC(CF_3)_3)_4]^-$ and $[Sb(OTeF_5)_6]^-$ anions are of comparable size (724 *vs.* 758 Å^3), we expect similar behaviour

Table 5 Solid state reaction enthalpies $\Delta_r H$ (s) in kJ mol^{-1}

Reaction	$\Delta_r H$ (s)
6 $Se_{grey\,(s)}$ + 2 $Ag[Sb(OTeF_5)_6]_{(s)}$ + 2 $SO_{2\,(l)}$ → $[(OSO)Ag(Se_6)Ag(OSO)][Sb(OTeF_5)_6]_{2\,(s)}$	–415
6 $Se_{grey\,(s)}$ + 2 $Ag[Sb(OTeF_5)_6]_{(s)}$ + 4 $SO_{2\,(l)}$ → $[(OSO)_2Ag(Se_6)Ag(OSO)_2][Sb(OTeF_5)_6]_{2\,(s)}$	–459
6 $Se_{grey\,(s)}$ + 2 $Ag[Sb(OTeF_5)_6]_{(s)}$ → $[Ag_2Se_6][Sb(OTeF_5)_6]_{2\,(s)}$	–291
6 $Se_{grey\,(s)}$ + 2 $Ag[Sb(OTeF_5)_6]_{(s)}$ → $Se_6[Sb(OTeF_5)_6]_{2\,(s,chair)}$ + 2 $Ag_{(s)}$	–214
6 $Se_{grey\,(s)}$ + 2 $Ag[Sb(OTeF_5)_6]_{(s)}$ → $Se_6[Sb(OTeF_5)_6]_{2\,(s,boat)}$ + 2 $Ag_{(s)}$	–238
6 $Se_{grey\,(s)}$ + 2 $Ag[Sb(OTeF_5)_6]_{(s)}$ → $Se_8[Sb(OTeF_5)_6]_2$ (s) + 2 $Ag_{(s)}$	–281

and did not additionally investigate the aluminate based reactions. The values for the reaction enthalpies $\Delta_r H$(s) in Table 5 show that **1** is more than 100 kJ mol^{-1}, and **2a** an additional 40 kJ mol^{-1} more favourable than all other suggested products (Se_6^{2+}, Se_8^{2+}). The influence of the entropy is neglected in this investigation, because it has only minor influence on the solid state estimations. This again shows that the formation of **1** and **2a** is induced by the high lattice potential energies of the respective dication salts $[(OSO)Ag(Se_6)Ag(OSO)][Sb(OTeF_5)_6]_2$ and $[(OSO)_2Ag(Se_6)Ag(OSO)_2][Al(OC(CF_3)_3)_4]_2$. The preference for the $[(OSO)Ag(Se_6)Ag(OSO)]^{2+}$ cation in **1** and $[(OSO)_2Ag(Se_6)Ag(OSO)_2]^{2+}$ in **2a** may be explained by the reaction environment: **1** crystallized from an oily residue left open in the atmosphere of a glove box and thus SO_2 was a minimum factor. In agreement with the Gibbs energies collected in Table 4 in solution, the addition of the second SO_2 molecule is even slightly endergonic and thus under the experimental conditions the excess SO_2 did probably escape into the atmosphere of the glove box. By contrast, crystals of **2a** were obtained in the presence of SO_2 solvent and were mounted on the diffractometer at low temperatures (–50 °C). Thus no possibility to escape the system was given and thus, in agreement with the solid state reaction enthalpy in Table 5, the SO_2 rich salt **2a** was formed.

Bonding considerations

All Ag–Se distances in **1**, **2a** and the $[Ag(Se_6)^+]_\infty$, stacks in **3** and **4** as well as in the calculated structures (Table 1 and Fig. 5) are in the same range (2.744–3.063 Å), but longer than the Ag2–Se–bonds linking the Se_6 rings in **4** (2.688(3) Å). The latter distance is similar to those in $(AgI)_2Se_6$ (2.686(2) Å) and the average distances found for silver selenides,[64] *e.g.*, 2.67(4) Å(ave) in $[(Ph_4P)Ag(Se_4)]_n$. Also the calculated fragments **B** and **C** show this bond shortening for Ag2–Se. This stronger bond induces a Se–Se bond lengths alternation in Se_6 similar to that found in $PdCl_2Se_6$ *via* $4p^2 \rightarrow \sigma^*$(Se–Se) interactions and slight lengthening of the Ag1–Se1 distance relative to the Se2–Ag1 bond (see Fig. 7/Table 1).

The Wiberg Bond Indices (WBI) support this picture (Se–Se 1.07 *vs.* 0.93) as well as NBO analysis with a significant donation from the Se $4p^2$-LP to the neighbouring σ*(Se–Se) orbital (S 4.3.2). All the Se–Se–Ag1 angles in **1–4** and the calculated structures are about 90° implying Se $4p^2$ electron pair donation in to the acceptor orbital of Ag^+, driven by Ag–Se bond formation and positive charges delocalization from Ag^+ to Se_6 (*cf.* IE: $Ag_{(g)}$ = 731, $Se_{6(g)}$ = 857 kJ mol^{-1}). Charge distribution to the selenium ring is found also with NPA and PABOON. While in the first the natural charges support clearly a charge separation Ag^+–Se_6 (Ag: 0.76, Se: 0.03/0.04), the PABOON multicentre charge is more

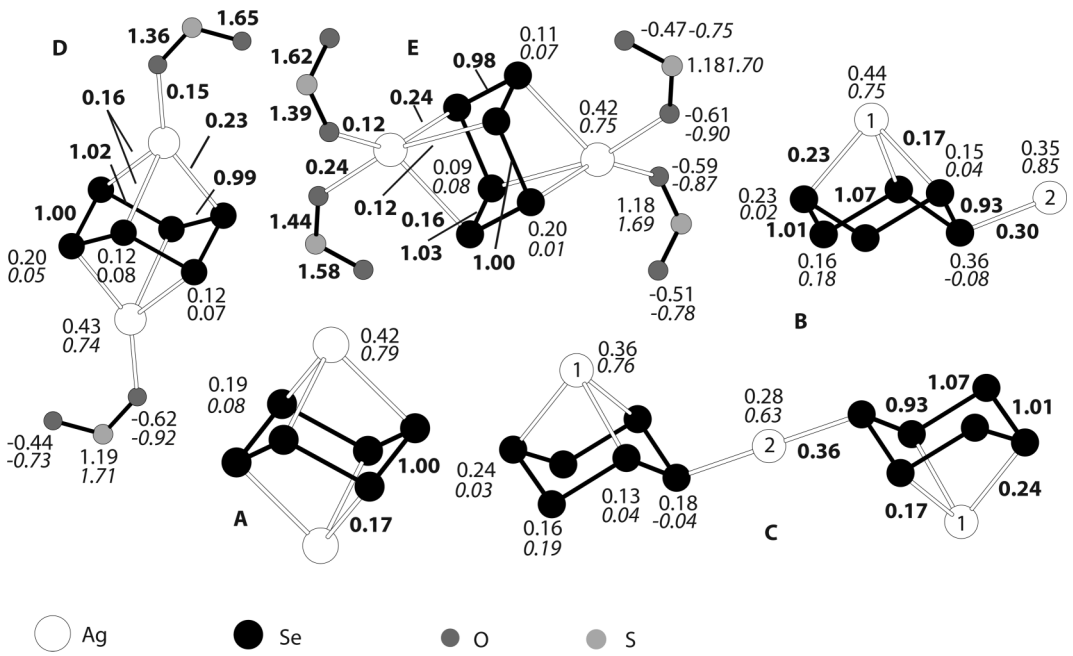

Fig. 7 Calculated structures A–E. Regular: Multicentre corrected PABOON (Population Analysis Based On Occupation Numbers) atom charges; *Italics*: NPA (Natural Population Analysis) natural charges; Bold: Wiberg Bond Indices (WBI).

evenly distributed over the atoms (Ag: 0.36, Se: 0.13–0.24). The observation of secondary Se–F contacts between the selenium atoms of the six membered rings and the fluorine atoms of the anions in **1** to **4** (See Table 1) gives evidence for relatively higher positive charge distribution to the selenium rings as suggested by the PABOON analysis. The silver atom Ag2 involved in the shortened Ag2–Se bond in **B** and **C** bears a more populated 5 s silver orbital (Natural Electron Configuration 5s(0.44) Ag2 *vs.* 5s(0.24) Ag1) and there are lower charges on Ag2 (0.28 PABOON/0.63 NPA) *vs.* Ag1 (0.36/0.76) (see Fig. 7).

The observed Se–Se bond alternation in **4** was verified by the calculated structures as well as population analyses (see Fig. 7). Due to the stronger Se1–Ag2 contacts (2.688(2) Å), the Se1–Ag1 (2.941(3) Å) and Se1–Se2 (2.362(2) Å) distances are longer than those in **1–3**. Also the higher WBI of 0.36 for the Se–Ag2 bond *vs.* 0.17 and 0.23 for the Se–Ag1 bonds reflects the influence of the strong Se–Ag2 contact. For Se2 directly neighbouring two silver atoms a special situation arises: it acts as a $4p^2$ electron pair donor to both Ag1 and Ag2 with a deviation of about 30° from the Se2–Ag2–Se2 angle (see Fig. 1d). If hybridization of 4 s and 4p orbitals is considered two lone pairs become available for donation with a much better overlap with the silver acceptor orbitals. The NBO analysis underlines this possibility; some core electron density from selenium (4 s) is donated to the Ag2 $5s^0$ orbital (S 4.3.2‡). A quantitative influence on Ag1 could only be given by a fragment with two additional Ag1 atoms, the calculation of which with a +5 charge is not sensible. Overall, the population analyses (particularly PABOON) and the Se–F contacts in the crystal structures suggest $4p^2 \rightarrow \sigma^*$charge delocalization over the entire 1D and 2D network.

Conclusion

Attempts to prepare $Se_6[A]_2$ ($[A]^-$ = $[Sb(OTeF_5)_6]^-$, $[Al(OC(CF_3)_3)_4]^-$) containing the hitherto unknown Se_6^{2+} dication, by the reaction of elemental selenium and $Ag[Sb(OTeF_5)_6]$ and bromine led to the formation of $[(OSO)Ag(Se_6)Ag(OSO)][Sb(OTeF_5)_6]_2$ **1**. Our attempts to prepare **1** directly from selenium and $Ag[Sb(OTeF_5)_6]$ were not successful, but the related compound $[(OSO)_2Ag(Se_6)Ag(OSO)_2][Al(OC(CF_3)_3)_4]_2$ **2a** was prepared from selenium and $Ag[Al(OC(CF_3)_3)_4]$. Reaction of $Ag[MF_6]$ (M═As,Sb) with elemental selenium lead to crystals of **3** and **4** containing unsolvated polymeric $[Ag(Se_6)^+]_\infty$ stacks that are additionally –Ag–$SeSe_4$SeAg– cross linked in **4**. The latter is best prepared by the reaction of $Se_4[AsF_6]_2$, silver metal and elemental selenium in the correct stoichiometric ratio according to equation 6. The PRESTO III sequence enabled us to obtain well resolved ^{109}Ag MAS NMR spectra of 3, 4, and the silver-fluorine containing compounds, AgF, AgF_2, $AgMF_6$ and $\{1/\infty[Ag(I_2)]_\infty\}[MF_6]$ (M = As, Sb). These are the first examples of ^{109}Ag MAS NMR spectra of fluorine containing compounds obtained in reasonable time and resolution scales.

The coordination polymers **3** and **4** may possess interesting physical properties *e.g.* electrical conductivity, which await future investigations.

It appears very likely that the aggregation behaviour of the Ag^+–Se_6 system is directly related to ion size: In compounds **1** and **2a** with very large anions (V_{anion} = 0.724[65] and 0.758[66] nm^3) the formation of Ag–Se_6 polymeric chains is not possible due to the smaller $[Ag_2Se_6]^{2+}$ building blocks. The coordination sphere of Ag^+ is saturated by Se_6 and SO_2. When the smaller $[Ag_2(SbF_6)_3]^-$ and $[AsF_6]^-$ anions are involved (V_{ion} ≈ 0.375 and 0.110 nm^3),[67] the reduced space requirement of the smaller anion allows for a polymeric packing. Thus, the soft Ag^+ acid seeks a preferred entirely *HSAB*-soft environment which is constructed from six Se atoms, and not the mixed hard-soft $Se_3O_xF_y$ arrangements in **1** and **2a**. Finally, the additional cross-linking in **4** is developed by the formation of again smaller $[Ag_2(SbF_6)_3]^-$ anion. This work suggests that the structurally hitherto uncharacterised $[Ag(Te_x)]^+$ cations (anions $[MF_6]^-$, M = As, Sb) are likely also polymeric.[68]

In all compounds, the polymeric spirals in grey selenium are converted into the metastable molecular cyclo Se_6 form. This new class of $[Ag(Se_6)]^+$ salts together with salts containing $[Ag(S_8)_n]^+$ (n = 1, 2), $[Ag(P_4)_n]^+$ (n = 1, 2) and $[Ag(I_2)^+]_n$ imply the emergences of a novel coordination chemistry of metal cation - electronegative element molecules. It is possible that elusive cations such as $[M(N_2)]^+$ (M = Na, K),[69] $[Au(X_2)]^+$ (X = Cl, Br),[70,71] $[Li(P_4)]^+$,[72] $[Ag(C_{60})]^+$,[73] and related $[M(NO)_x]^+$ (M = Ag, Cu; x = 1, 2),[74–77] which have been detected in gas phase, may one day be isolated on the preparative scale with suitable weakly coordinating anions.

The Se_6 rings in all the silver complexes are all positively charged and partially oxidised. As possible intermediates they may provide a safer route to homopolyatomic cations. Previously, those were synthesized by reactions of strong oxidation agents, *e.g.* MF_5 (M = As, Sb) and $S_2O_6F_2$, with the corresponding element or *via* solid state methods. However the experimental findings and an analysis of the energetics of the system showed that in the solid state the Ag–Se_6 complexes were favoured over the pure selenium cations. The neutral Se_6[78–80] may be displacable from these salts on addition of a stronger base, assuming that Se_6 is not converted to thermodynamically stable Se_8 or grey Se_∞. This was observed in preliminary experiments by addition of acetonitrile as a base to $[Ag(Se_6)]$-containing solutions that will be reported elsewhere.

Experimental section

General techniques

General techniques and methods have been described elsewhere.[81] Reactions were carried in a two bulb (Pyrex, 25 ml), two valve (Teflon in glass, o.d. 0.5 cm) vessel, or a two tube (Pyrex, o.d. 1.5 cm, length 10 cm), two valve (Teflon in glass, o.d. 0.8 cm) vessel, incorporating a medium frit and a Teflon coated stirring bar magnet. All vessels were carefully flame dried *in vacuo* prior to use. Moisture-sensitive materials and all solid products were manipulated in a Vacuum Atmospheres Dri-Lab equipped with a Dri train (HE-493) and an internal circulating drying unit containing one kg of 3 Å molecular sieves or in Argon filled Glove Boxes (M. BRAUN) with O_2 and H_2O content below 1 ppm. Chemical analyses were performed by Galbraith Laboratories, Inc. and at the Institut für Anorganische Chemie, Friedrich Wilhelms Universität (Bonn). FT-IR spectra of Nujol mulls between KBr disks were recorded on a Thermo Nicolet FT IR 470 spectrometer (32 scans; resolution, 2.0 cm^{-1}). FT-Raman spectra were recorded on a Bruker IFS66 FT-IR spectrometer equipped with a Bruker FRA106 FT-Raman accessory using a Nd: YAG laser (emission wavelength, 1064 nm; maximum laser power, 3009 mW). Samples

were sealed in melting point capillaries, and data were collected in the backscattering mode (180° excitation). Raman spectra of **2a** were recorded using a Bruker Vertex 70 equipped with a RAM II module using a 1064 nm Nd:YAG laser source in 180° backscattering mode.

Chemicals

Silver powder (99.995, Alfa Aesar), Grey selenium powder (99%, BDH Chemicals and 99.7% Aldrich (**2a/b**) and selenium pellets (99.999+%, ~ 2 mm, Aldrich) were used without further purification. $Ag[SbF_6]$ (SynQuest. Labs. Inc.) was dissolved in liquid SO_2 and the insoluble portion removed by filtration. $Ag[AsF_6]$,[82] $Se_4[AsF_6]_2$[81] and $Ag[Al(OC(CF_3)_3)_4]$[83] were prepared as described.

The purity of $AgMF_6$ (M = As, Sb) was confirmed by FT-Raman spectroscopy. $AgSbF_6$ (Acros), AgF (Merck), and AgF_2 (Riedel, >98%) were used for ^{109}Ag solid state NMR measurements without further purification. $(AgI_2)MF_6$ (M = As, Sb) was prepared according to literature procedures.[23] SO_2 (BOC Canada Ltd.) and SO_2ClF (Matheson) were distilled onto and stored over CaH_2 or molecular sieves (4 Å) respectively at least 24 h prior to use. CH_2Cl_2 (99.5% min., Anachemia Science) was stirred over P_2O_5 for two days and then distilled onto and stored over CaH_2 at least 24 h prior to use. F-114 ($Cl_2FC\text{-}CFCl_2$, Matheson) was distilled onto and stored over molecular sieves 3 Å at least 48 h prior to use. Teflic acid, F_5TeOH, was prepared from Oleum, NaF and $Te(OH)_6$ by a modification of the literature method.[84]

Preparation of $AgOTeF_5$

Preparation of $AgOTeF_5$ followed the published method (AgF + $HOTeF_5$ in CH_2Cl_2).[85] However, in our hands it was impossible to remove all traces of the solvent CH_2Cl_2 by subjecting the purified $AgOTeF_5$ over night to a dynamic vacuum. This was shown by the ^{1}H-NMR spectrum of a sample of $AgOTeF_5$ dissolved in SO_2, which showed one line at δ^1H = 5.23 ppm [*cf.* $\delta^1H(CH_2Cl_2)$ = 5.30 ppm in $CDCl_3$].[86] The ^{19}F-NMR shifts of the AB_4 spin system of $AgOTeF_5$ in SO_2 were not reported previously and are $\delta^{19}F$ = –27.7 ppm (1F, quint., F_A) and –38.5 ppm (4F, d, F_B) with $^2J(^{19}F_A\text{–}^{19}F_B)$ = 180.0 Hz.

Preparation of $Ag[Sb(OTeF_5)_6]$

In our hands we were unable to prepare $Ag[Sb(OTeF_5)_6]$ free of CH_2Cl_2 by the published procedures.[41] However we were able to markedly reduce the impurity by the use of F-114/SO_2 as a solvent, and the resulting $Ag[Sb(OTeF_5)_6]$ was used in our reactions below. A full account is given in the supplementary material.‡

Solution NMR

Solution NMR spectra were obtained of samples in 10 mm (o.d.) thick walled NMR tubes fitted by a J. Young valve. They were recorded between –70 °C and r.t. on a variable temperature, multinuclear Varian Associates Unity 400 spectrometer and were referenced against external TMS ($CDCl_3$, ^{1}H), $CDCl_3$ (neat, ^{13}C), $FCCl_3$ (SO_2, ^{19}F), Me_2Se (neat, ^{77}Se), and SbF_6^- (aqueous, ^{121}Sb) as a standard (r.t.). The solution NMR spectra of **2a** were recorded on a Bruker Avance II+ 400 WB spectrometer at 25 °C and –40 °C in 5 mm NMR tubes fitted by a J. Young valve.

Solid-state NMR

The ^{109}Ag and ^{19}F solid state NMR experiments were carried out on a Varian Infinity spectrometer equipped with a commercial 4 mm MAS NMR triple-resonance probe utilizing a low-gamma extension box for the ^{109}Ag channel. The magnetic field strength was 9.4 T corresponding to a ^{109}Ag and ^{19}F resonance frequency of 18.68 and 377.81 MHz, respectively. The ^{109}Ag MAS NMR spectra were acquired using the PRESTO-III experiment. Those are non-quantitative with respect to the ratio of peak intensities. The PRESTO-III pulse sequence is described in detail in reference.[57] The spectra shown have been acquired in typically 2–6 h with a repetition delay of 5 s at room temperature and continuous wave ^{19}F decoupling. The nutation frequency for the hard pulses on the ^{109}Ag channel was 31 kHz. At 12 kHz spinning frequency the ^{19}F nutation frequency used for the $R18_2^5$ amounts to 54 kHz. The transfer times τ_1 and τ_2 were optimised on the sample and typically set to values around 5.333 ms. The ^{109}Ag chemical shifts refer to a solution of 9 M $AgNO_3$ + 0.25 M $Fe(NO_3)_3$ in H_2O and the ^{19}F chemical shifts to $CFCl_3$. All experiments were carried out at room temperature.

Reaction of $Ag[Sb(OTeF_5)_6]$ with grey Se leading to dissolved $Se_{10}[Sb(OTeF_5)_6]_2$

Grey Se powder (0.189 g, 2.394 mmol) and 1.048 g beige $Ag[Sb(OTeF_5)_6]$ (0.631 mmol) were carefully ground together for about five minutes and the resulting light grey material loaded into a two-bulb frit-plate vessel equipped with a specially designed NMR-outlet to allow the preparation of NMR samples.[65] The mixture was ultrasonicated at *ca.* 30 °C for 3–4 hs giving an intensely brownish/black product to which 11.86 g of SO_2 was added giving a deep brown solution which was filtered and a portion was poured into a 10 mm (o.d.) NMR tube (4.64 g solution). The ^{77}Se-NMR spectra of this sample (r.t., –30 °C and –70 °C) showed lines at $\delta^{77}Se$ = 1103 and 766 ppm as well as those attributable to Se_8^{2+} (only –70 °C) characteristic of Se_{10}^{2+} [reversible low temp. disproportionation to Se_8^{2+} and Se_{17}^{2+}]. 0.58 g of a dark brown solid were recovered which had a very poor FT-Raman spectrum (strong fluorescence). 24 h later the FT-Raman showed small amounts of elemental selenium and an isolated weak C–H stretch at 2860 cm^{-1}. A similar decomposition behavior of the Se_{10}^{2+} cation was reported.[39] Similar experiments reacting Se and $Ag[Sb(OTeF_5)_6]$ in SO_2 solution designed to prepare $[Se_x][Sb(OTeF_5)_6]$ (x = 6, 8) led to a mixture of Se_8^{2+} and Se_{10}^{2+} (^{77}Se NMR at –70 °C, SO_2 as solvent). Details are given in the supplementary material (S6).‡

Reaction leading to single crystals of 1

41.33 g of F-114 was condensed onto grey Se (0.180 g, 2.280 mmol), Se_2Br_2 [prepared by heating Se (0.159 g, 2.016 mmol) and Br_2 (0.167 g, 1.042 mmol) for 1–2 min to *ca.* 100 °C] and solid $Ag[Sb(OTeF_5)_6]$ (2.510 g, 1.511 mmol). The resulting suspension was stirred over night. It appeared that no reaction had occurred, therefore SO_2 (1.45 g) was added. On warming to 5 °C, the solution turned dark green (colour of Se_8^{2+}), within 5 to 10 mins but after 15 min only a yellow-beige precipitate over a light yellow solution remained. Stirring over night at +5 °C, filtration and removal of the solvent resulted in the separation of a few drops of a yellow-orange

oil from the solution, which was washed back into the reaction bulb and the volatiles removed *in vacuo* (1.5 h at HV). 17.92 g of SO_2 were condensed onto the yellow-beige solid material, giving a fine precipitate (colourless, AgCl?) and a clear yellow-orange coloured solution. Filtering this solution into the second bulb (at +5 °C) and cooling the first bulb to 0 °C afforded needle like yellow crystals. These were isolated by pouring the supernatant solution back into the reaction bulb and removing all the volatiles in vacuo, leaving a large amount of a yellow-orange oil. This vessel was cut open in the dry box to isolate the crystals (0.737 g) [This material showed strong fluorescence in the FT-Raman spectrum; no ^{77}Se NMR spectrum at r.t. and −70°, 0.32 g in SO_2, 3000 scans]. Upon addition of acetonitrile to these SO_2 solutions the immediate precipitation of a red substance was observed (red selenium?). Large yellow-orange cube like crystals grew from the remaining oil in the second bulb with its valve closed in the dry box after 3 months. An X-ray crystal structure determination of one of the multitude of very similar appearing crystals showed it to be **1**.

Preparation of single crystals 2a and bulk 2b

Liquid SO_2 (20 ml) was condensed onto a mixture of grey selenium (0.88 g, 11.14 mmol) and pale yellow $Ag[Al(OC(CF_3)_3)_4]$ (2.00 g, 1.91 mmol) (molar ratio 6 : 1) in a two bulbed Schlenk vessel with Young (J. Young, London) valves with a G4 frit in between. The reaction mixture can either be stirred for several days or sonicated for 6 h until the reaction mixture turns yellow-orange. The reaction progress can be monitored by colour changes. First the mixture turns green (indicating possible selenium cations), later on orange (formation of the complex). The mixture was filtered into the second bulb, giving a clear solution; remaining greyish residues were confirmed to be grey selenium by powder diffraction (ESI S9‡). The solution was concentrated until an orange oil remained and crystallized using the published "oil technique".[87] **2a** crystallised at 2 °C within two days yielding orange crystals sensitive towards light and atmosphere. Upon removal of the remaining solvent 1.65 g (theory for 100% yield based on eqn (2): 2.44 g) of an orange powder was obtained **2b**. No peaks attributable to (coordinated) SO_2 were visible in the IR of the orange powder: IR(ZnSe-ATR): 1355(w), 1299(sh), 1240 (s), 1211 (s), 1176 (s), 1128 (sh), 968 (vs), 862 (w), 831 (w), 796 (w), 725 (s) cm^{-1}. NMR(SO_2, 298 K): ^{19}F ($[Al(OC(CF_3)_3)_4]^-$ −75.3 ppm), ^{27}Al ($[Al(OC(CF_3)_3)_4]^-$ 34.6 ppm), ^{77}Se (unassigned, see ESI S9‡).

Preparation of single crystals of 3 and 4

About 30 ml SO_2 was condensed onto a mixture of $Ag[MF_6]$ (M = Sb (**3**) 1.0 g, As (**4**) 4.35 g) and selenium powder (M = Sb 0.044 g, M = As 0.1 g) in one tube of a standard two bulb, two-valve vessel (H vessel)[88] fitted with a medium porosity frit and a magnetic stirring bar. On warming to r.t. orange (**3**) and yellow (**4**) solutions were formed and immediately filtered without washing. Small amounts of orange (**3**) or yellow crystals were given after a few minutes at r.t.. The H-vessel was cooled to −78 °C and one valve was opened under argon. The crystals were picked out of the solution by using a miniature nickel spoon. One crystal suitable for X-ray crystal structure analysis was chosen and quickly placed in the fluorinated oil cooled in a stream of liquid nitrogen and examined under the microscope. The crystal was mounted in the end of a glass needle and placed into liquid nitrogen, and then into the cold N_2 stream of the diffractometer. By this method small quantities of crystals of **3** and **4** were isolated.

Reactions leading to bulk 4, method 1: reactions of $Ag[AsF_6]$ with Se pellets

Liquid SO_2 (15.665 g) was condensed onto $AgAsF_6$ (1.315 g, 4.431 mmol) and Se pellets (0.164 g, 2.077 mmol) in one bulb of a two-bulb vessel. A bright yellow solution above the unreacted Se pellets was observed after stirring for two hours. The size of the Se pellets reduced after stirring for two days with formation of a bright yellow solid under a yellow solution. The insoluble (Se and yellow product) and soluble materials were separated by repeated washings (5 times) across the frit. The solvent was removed giving 0.222 g (calc. 0.245 g, based on equation 5 above) of a yellow insoluble product separately manually from 0.055 g unreacted Se pellets and 1.131 g unreacted $AgAsF_6$ (calc. 1.265 g). Thus the ratio of Se : $Ag[AsF_6]$ reacted was about 3 : 1. Elemental analysis calcd (%): Se 44.39, Ag 20.21, As 14.04; found: Se 43.4, Ag 20.6, As 14.6). In a related reaction of Se pellets (1.965 g, 24.886 mmol) reacted with $Ag[AsF_6]$ (0.934 g, 3.147 mmol) (molar ratio: Se/$AgAsF_6$ = 8 : 1) for 24 days in which time all $Ag[AsF_6]$ was consumed giving 1.210 g (cal. 1.214 g based on all reacted $Ag[AsF_6]$) and 1.689 g (calc.1.679 g) yellow product. The ratio of reacted Se: $AgAsF_6$ was 3 : 1. Elemental analysis calcd (%): Se 44.39, Ag 20.21, F 21.36, As 14.04; Found: Se 44.47, Ag 19.85, F 21.46, As 14.57. The frequencies of FT-IR and FT-Raman for the yellow product from these two reactions are included in ESI Table 1.2, and its FT-Raman spectrum is shown in ESI Figure S3.‡ Other reactions of $Ag[MF_6]$ (M = As, Sb) with Se (powder and pellets) together with these two reactions are summarized in Table S1.1.‡ Corresponding reaction weights, FT-IR data, FT-Raman data and X-ray powder fraction patterns were given in the supplementary material (ESI S1.3–S1.7‡). The X-ray powder pattern calculated from the single crystal data of **4** was in good agreement with the experimental X-ray powder data (ESI 1.8‡) and the ^{109}Ag MAS NMR gave two ^{109}Ag resonances in agreement with the structure of **4** (Table 3).

Method 2: reaction of $Se_4[AsF_6]_2$ with the Ag metal and the Se powder (mole ratio: 1 : 2 : 2)

Liquid SO_2 (about 10 g) was condensed onto a mixture of yellow-green $Se_4[AsF_6]_2$ (0.693 g, 0.999 mmol), black Se powder (0.152 g, 1.925 mmol) and silver (0.213 g, 1.975 mmol) in one bulb of a two bulb vessel. The reaction was stirred at room temperature for 15 days. The yellow solution was filtered and the insoluble yellow material was washed five times with SO_2. Removal of SO_2 gave a yellow insoluble product (1.003 g, calcd. 1.058 g based on equation 5 above). Elemental analysis calcd (%): Se 44.39, Ag 20.21, As 14.04; found: Se 43.0, Ag 21.4, As 14.3. The Raman spectrum and X-ray powder diffraction pattern (ESI S1.8‡) of the yellow insoluble product were identical to that from method 1.

X-ray crystal structure determinations

1: Crystals suitable for X-ray crystal structure determination were examined in the dry box by an externally mounted stereomicroscope (Leitz, magnification 6,18 and 40×) of long focal length.

Table 6 Crystallographic and refinement details

Compound	**1**	**2a**	**3**	**4**
Formula	$Ag_2Se_6S_2O_{16}Sb_2Te_2F_{60}$	$Ag_2Se_6S_4O_8Al_2O_8C_{32}F_{72}$	$Ag_3Se_6Sb_3F_{18}$	$AgSe_3AsF_6$
Formula weight	3924.32	1440.01	1504.62	533.67
Crystal system	Cubic	Triclinic	Monoclinic	Monoclinic
Space group	$Pa\bar{3}$	$P\bar{1}$	$C2/c$	$C2/m$
a/Å	19.1532(2)	10.639(2)	21.821(5)	9.284(9)
b/Å	19.1532(2)	13.638(3)	10.748(3)	15.491(7)
c/Å	19.1532(2)	13.834(3)	10.718(3)	5.290(2)
α/°	90	71.06(3)	90	90
β/°	90	78.05(3)	119.113(3)	92.41(10)
γ/°	90	86.37(3)	90	90
V/Å^3	7026.3(1)	1857.5(6)	2196.2(10)	760.1(9)
Z	4	2	4	4
ρ_c/g cm^{-3}	3.710	2.575	4.550	4.663
T/K	213(1)	110(1)	173(1)	173(1)
Abs. corr.	SADABS	Multi-scan empirical	SADABS	SADABS
Refl. obs. ($I > 3\sigma$)	2069	5792	1890	693
GOOF	1.185	1.087	1.095	0.846
Final $R1$ ($I > 2\sigma$)	0.0501	0.1104	0.0381	0.0322
Final $wR2$	0.0852	0.3321	0.0957	0.0483

Selected crystals were placed in rigorously dried capillary tubes and sealed under an atmosphere of dry nitrogen as previously described.[89] Crystals were mounted on a Siemens P4 diffractometer equipped with a SMART CCD detector. Frames were collected at 213 ± 1 K with an exposure time of 10 s and a scan range of 0.31° per frame. Data were corrected for Lorentz, polarization and absorption effects. The structure was solved by direct methods and refined by full matrix least squares refinement on F^2. All atoms were refined anisotropically. Structure solution and refinement was performed using the Siemens SHELXTL-Plus software package.[90]

2a: Crystals were selected and prepared at 253 K in Perfluoroetheroil (ABCR), then mounted with a CRYOLOOP (Hampton Research) on a Rigaku R-Axis Spider diffractometer equipped with a Curved Image Plate detector. The frames were collected using Mo-Kα-radiation (0.71073 Å) at T = 110(2) K (Oxford Cryostream 700) with an exposure time of 6 min (2Θ limited to 60°). Cell refinement, data reduction, Lorentz, polarization and empirical absorption correction as well as integration were carried out with the CRYSTALCLEAR[91] software utilizing the FSPROCESS[92] routine.

The structure was solved with the Patterson method (SHELXS97[93]), and then refined stepwise by full matrix least squares refinement on F^2 with SHELXL97.[93] The data was limited using SHEL 999 0.875. The disorder in the anion for both -CF_3 and $C(CF_3)_3$-groups was refined anisotropically for the major site occupation and isotropically for the minor site occupation. The minor occupied disordered CF_3-groups were restrained using the SAME command, major occupied groups using the SADI command. N.P.D atoms where made isotropically using the ISOR command.

3 and **4**: Crystals were mounted on a Bruker AXS P4 diffractometer with SMART 1000 detector, frames were collected at 173 ± 1 K. Data were corrected for Lorentz, polarization and absorption effects.

All relevant data referring to crystallography, data collection and refinement compiled in Table 6. Further details on the crystal structure determinations are deposited at the Fachinformationszentrum, Karlsruhe, Germany and may be requested by quoting the depositing number CSD-418699 (**1**), 418700 (**3**), and 418701 (**4**). The structure of **2a** is deposited at the Cambridge Crystal Data Centre (CCDC) and may be requested by quoting the depositing number CCDC-814799. The graphical representations were prepared with DIAMOND.[94]

Computational details

All structures were investigated at the DFT BP86[95]/def-SV(P)[96,97] and hybrid-DFT PBE0[98–100]/def2-TZVPP[101] levels with a 28 electron ECP on silver.[102] The calculations were carried out with the TURBOMOLE[103] V6.0 program package assuming the highest possible point group for each compound. Each optimised structure proved to be a minimum utilizing the AOFORCE module. If not otherwise stated no imaginary frequencies were found. Additional calculations were performed at the MP2/def2-TZVPP level with the resolution-of-the-identity and frozen core approximation.[104,105] For the numerical calculation of vibrational frequencies the module NUMFORCE was used. Polarization tensors and their projection to the normal vibrational modes were calculated either by the module RAMAN or with both EGRAD and INTENSE. Enthalpies are calculated for 0 K or corrected to 298.15 K using the FreeH module with scaling factors (0.9833 for BP86/SV(P) and 0.97[106] for PBE0/def2-TZVPP). To take solvent effects into account single point calculations on the optimised geometries were performed using the COSMO model with ε_r = 16.3[52] (SO_2, T = 298 K). Population Analysis Based On Occupation Numbers[107,108] was accomplished. Full NBO analysis has been carried out as a single point calculation using PBE0/def2-TZVPP with GAUSSIAN03 (Rev. E.01).[109]

Acknowledgements

This work was supported by the Natural Science and Engineering Research council of Canada NSERC (J. P.). I. K. is grateful to the Alexander von Humboldt Foundation in Bonn, Germany, for providing a Feodor-Lynen Fellowship. J. S. a. d. G gratefully acknowledges financial support by the Deutsche

Forschungsgemeinschaft through the Emmy–Noether program. We are indebted to Dr James F. Britten at McMaster University, Hamilton, Canada for collecting the X-ray data set for **1**. T. K and I. K. thank Prof. C. Röhr for helpful discussions, and Ines Dürr and Stefanie Haseloff for recording the PXRD.

References

1 R. Steudel, *Angew. Chem.*, 1975, **87**, 683–692.
2 R. Steudel, *Top. Curr. Chem.*, 1982, **102**, 149–176.
3 R. Steudel, M. Pridoehl, H. Hartl and I. Bruedgam, *Z. Anorg. Allg. Chem.*, 1993, **619**, 1589–1596.
4 R. Steudel, O. Schumann, J. Buschmann and P. Luger, *Angew. Chem., Int. Ed.*, 1998, **37**, 2377–2378.
5 R. Steudel and E. M. Strauss, *Adv. Inorg. Chem.*, 1984, **28**, 135–166.
6 A. Goldbach, L. Iton, M. Grimsditch and M.-L. Saboungi, *J. Phys. Chem. B*, 1997, **101**, 330–334.
7 V. V. Poborchii, *Chem. Phys. Lett.*, 1996, **251**, 230–234.
8 G. Wirnsberger, H. P. Fritzer, R. Zink, A. Popitsch, B. Pillep and P. Behrens, *J. Phys. Chem. B*, 1999, **103**, 5797–5801.
9 J. Beck, *Angew. Chem., Int. Ed. Engl.*, 1994, **33**, 163–172.
10 J. Beck, *Coord. Chem. Rev.*, 1997, **163**, 55–70.
11 J. Beck, ed., *Inorganic Chemistry in Focus II*, Wiley-VCH, Weinheim, 2005.
12 S. Brownridge, I. Krossing, J. Passmore, H. D. B. Jenkins and H. K. Roobottom, *Coord. Chem. Rev.*, 2000, **197**, 397–481.
13 N. Burford, J. Passmore and J. C. P. Sanders, ed., *From Atoms to Polymers, Isoelectronic Analogies*, 1989.
14 R. J. Gillespie, *Chem. Soc. Rev.*, 1979, **8**, 315–352.
15 R. J. Gillespie and J. Passmore, *Adv. Inorg. Chem. Radiochem.*, 1975, **17**, 49.
16 I. Krossing, ed., *Homoatomic Sulfur Cations*, Springer, Berlin, 2003.
17 J. Passmore, ed., *The Chemistry of Inorganic Ring Systems*, 1992.
18 H. W. Roesky, M. Thomas, J. Schimlowiak, P. G. Jones, W. Pinkert and G. M. Sheldrick, *J. Chem. Soc., Chem. Commun.*, 1982, 895–896.
19 T. S. Cameron, A. Decken, I. Dionne, M. Fang, I. Krossing and J. Passmore, *Chem.–Eur. J.*, 2002, **8**, 3386–3401.
20 A. Bihlmeier, M. Gonsior, I. Raabe, N. Trapp and I. Krossing, *Chem.–Eur. J.*, 2004, **10**, 5041–5051.
21 I. Krossing and L. Van Wüllen, *Chem.–Eur. J.*, 2002, **8**, 700–711.
22 I. Krossing, *J. Am. Chem. Soc.*, 2001, **123**, 4603–4604.
23 T. S. Cameron, J. Passmore and X. Wang, *Angew. Chem., Int. Ed.*, 2004, **43**, 1995–1998.
24 I. Raabe, S. Antonijevic and I. Krossing, *Chem.–Eur. J.*, 2007, **13**, 7510–7522.
25 A. Adolf, M. Gonsior and I. Krossing, *J. Am. Chem. Soc.*, 2002, **124**, 7111–7116.
26 W. A. S. Nandana, J. Passmore and P. S. White, *J. Chem. Soc., Chem. Commun.*, 1983, 526–528.
27 W. A. S. Nandana, J. Passmore, P. S. White and C. M. Wong, *Inorg. Chem.*, 1989, **28**, 3320–3328.
28 R. Faggiani, R. J. Gillespie, J. Kolis and K. C. Malhotra, *J. Chem. Soc., Chem. Commun.*, 1987, 591–592.
29 R. Faggiani, R. J. Gillespie and J. W. Kolis, *J. Chem. Soc., Chem. Commun.*, 1987, 592–593.
30 K. Neininger, H. W. Rotter and G. Thiele, *Z. Anorg. Allg. Chem.*, 1996, **622**, 1814–1818.
31 H.-J. Deiseroth, M. Wagener and E. Neumann, *Eur. J. Inorg. Chem.*, 2004, 4755–4758.
32 A. Bacchi, W. Baratta, F. Calderazzo, F. Marchetti and G. Pelizzi, *Inorg. Chem.*, 2002, **41**, 3894–3900.
33 A. Bacchi, W. Baratta, F. Calderazzo, F. Marchetti and G. Pelizzi, *Angew. Chem.*, 1994, **106**(2), 206–207 (See also *Angew. Chem., Int. Ed. Engl.*, 1994, **33**(2), 193–195).
34 P. Y. Demchenko, R. E. Gladyshevskii, S. V. Volkov, O. G. Yanko, L. B. Kharkova, Z. A. Fokina and A. A. Fokin, *Chem. Commun.*, 2010, **46**, 4520–4522.
35 M. Wachhold and M. G. Kanatzidis, *J. Am. Chem. Soc.*, 1999, **121**, 4189–4195.
36 M. Wachhold and W. S. Sheldrick, *Z. Naturforsch., B: Chem. Sci.*, 1997, **52**, 169–175.
37 W. S. Sheldrick and M. Wachhold, *Angew. Chem., Int. Ed. Engl.*, 1995, **34**, 450–451.
38 P. C. Shrivastava, *Indian J. Chem.*, 1990, **29A**, 75.
39 R. C. Burns, M. J. Collins, R. J. Gillespie and G. J. Schrobilgen, *Inorg. Chem.*, 1986, **25**, 4465–4469.
40 H. P. A. Mercier, J. C. P. Sanders and G. J. Schrobilgen, *J. Am. Chem. Soc.*, 1994, **116**, 2921–2937.
41 D. M. Van Seggen, P. K. Hurlburt, O. P. Anderson and S. H. Strauss, *Inorg. Chem.*, 1995, **34**, 3453–3464.
42 D. Aris, J. Beck, A. Decken, I. Dionne, I. Krossing, J. Passmore, E. Rivard, F. Steden and X. Wang, *Phosphorus, Sulfur Silicon Relat. Elem.*, 2004, **179**, 859–863.
43 B. Kesanli, J. Fettinger and B. Eichhorn, *Angew. Chem., Int. Ed.*, 2001, **40**, 2300–2302.
44 I. D. Brown, ed., *Structure and Bonding in Crystals*, Academic Press, London, 1981.
45 I. D. Brown, *The Chemical Bond in Inorganic Chemistry (The Bond Valence Model)*, Oxford University Press, Oxford, 2002.
46 A. Decken, C. Knapp, G. B. Nikiforov, J. Passmore, J. M. Rautiainen, X. Wang and X. Zeng, *Chem.–Eur. J.*, 2009, **15**, 6504–6517.
47 A. F. Wells, *Structural Inorganic Chemistry*, 5 edn, Clarendon Press, Oxford, 1984.
48 F. A. Cotton, E. V. Dikarev and M. A. Petrukhina, *Angew. Chem., Int. Ed.*, 2001, **40**, 1521–1523.
49 Y. Miyamoto, *Jpn. J. Appl. Phys.*, 1980, **19**, 1813–1819.
50 The analytical vibrational analysis leads to two imaginary frequencies of −6.75 and −5.32 cm^{-1} which are maybe an artefact of the DFT calculation.
51 A. Klamt and G. Schueuermann, *J. Chem. Soc., Perkin Trans. 2*, 1993, 799–805.
52 D. R. Lide, *CRC Handbook of Chemistry and Physics*, 83 edn, CRC Press, Boca Raton, 2002.
53 K. Nagata, K. Ishibashi and Y. Miyamoto, *Jpn. J. Appl. Phys.*, 1980, **19**, 1569–1570.
54 K. Nagata, K. Ishibashi and Y. Miyamoto, *Fukuoka Daigaku Rigaku Shuho*, 1980, **10**, 53–59.
55 A. L. Geddes and G. L. Bottger, *Inorg. Chem.*, 1969, **8**, 802–807.
56 D. Rappoport and F. Furche, *J. Chem. Phys.*, 2007, **126**, 201104/201101–201104/201105.
57 X. Zhao, W. Hoffbauer, J. Schmedt auf der Günne and M. H. Levitt, *Solid State Nucl. Magn. Reson.*, 2004, **26**, 57–64.
58 G. H. Penner and W. Li, *Inorg. Chem.*, 2004, **43**, 5588–5597.
59 H. Looser and D. Brinkmann, *J. Magn. Reson.*, 1985, **64**, 76–80.
60 The $\Delta G'_{solv}$ value calculated with COSMO is not the transfer from the ideal gas (1 atm) to 1 molar solution, so that the chemical potential difference $\Delta G'_{solv} \rightarrow \Delta G^{0}_{solv}$ of 7.93 kJ mol^{-1} has to be added.).
61 A. Baumann and J. Beck, *Z. Anorg. Allg. Chem.*, 2004, **630**, 2078–2082.
62 J. Beck and F. Steden, *Acta Crystallogr., Sect. E: Struct. Rep. Online*, 2003, **59**, i158–i160.
63 N. Wiberg, *Holleman Wiberg Lehrbuch der Anorganischen Chemie*, 102 edn, Walther de Gruyter, Berlin, 2007.
64 S. P. Huang and M. G. Kanatzidis, *Inorg. Chem.*, 1991, **30**, 1455–1466.
65 T. S. Cameron, I. Krossing and J. Passmore, *Inorg. Chem.*, 2001, **40**, 4488–4490.
66 I. Krossing, H. Brands, R. Feuerhake and S. Koenig, *J. Fluorine Chem.*, 2001, **112**, 83–90.
67 H. D. B. Jenkins, J. Passmore and L. Glasser, *Inorg. Chem.*, 1999, **38**, 3609–3620.
68 I. Dionne, *PhD Thesis*, University of New Brunswick, 2002.
69 H.-J. Himmel and M. Reiher, *Angew. Chem., Int. Ed.*, 2006, **45**, 6264–6288.
70 D. Schröder, R. Brown, P. Schwerdtfeger, X.-B. Wang, X. Yang, L.-S. Wang and H. Schwarz, *Angew. Chem., Int. Ed.*, 2003, **42**, 311–314.
71 H. Schwarz, *Angew. Chem., Int. Ed.*, 2003, **42**, 4442–4454.
72 J. L. M. Abboud, I. Alkorta, J. Z. Davalos, J. F. Gal, M. Herreros, P. C. Maria, O. Mo, M. T. Molina, R. Notario and M. Yanez, *J. Am. Chem. Soc.*, 2000, **122**, 4451–4454.
73 J. E. Reddic, J. C. Robinson and M. A. Duncan, *Chem. Phys. Lett.*, 1997, **279**, 203–208.
74 D. Suelzle, H. Schwarz, K. H. Moock and J. K. Terlouw, *Int. J. Mass Spectrom. Ion Processes*, 1991, **108**, 269–272.
75 T. W. Hayton, P. Legzdins and W. B. Sharp, *Chem. Rev.*, 2002, **102**, 935–991.
76 K. Koszinowski, D. Schröder, H. Schwarz, M. C. Holthausen, J. Sauer, H. Koizumi and P. B. Armentrout, *Inorg. Chem.*, 2002, **41**, 7170.
77 K. Koszinowski, D. Schröder, H. Schwarz, M. C. Holthausen, J. Sauer, H. Koizumi and P. B. Armentrout, *Inorg. Chem.*, 2002, **41**, 5882–5890.

78 G. B. Abdullayev, Y. G. Asadov and K. P. Mamedov, ed., *The Physics of Selenium and Tellurium*, Pergamon, London, 1969.
79 Y. Miyamoto, *Fukuoka Daigaku Rigaku Shuho*, 1977, **7**, 87–93.
80 Y. Miyamoto, *Jpn. J. Appl. Phys.*, 1977, **16**, 2257–2258.
81 M. P. Murchie, R. Kapoor, J. Passmore, G. Schatte and T. Way, *Inorg. Synth.*, 1997, **31**, 102–112.
82 H. W. Roesky and M. Witt, *Inorg. Synth.*, 1986, **24**, 72–76.
83 I. Krossing, *Chem.–Eur. J.*, 2001, **7**, 490–502.
84 I. Dionne, I. Krossing, J. Passmore, publication in progress.
85 S. H. Strauss, M. D. Noirot and O. P. Anderson, *Inorg. Chem.*, 1985, **24**, 4307–4311.
86 M. Hesse, M. Meier and B. Zeeh, *Spektroskopische Methoden in der Organischen Chemie*, 4 edn, Georg Thieme Verlag, Stuttgart, 1991.
87 I. Krossing and A. Reisinger, *Coord. Chem. Rev.*, 2006, **250**, 2721–2744.
88 J. Beck, F. Steden, A. Reich and H. Fölsing, *Z. Anorg. Allg. Chem.*, 2003, **629**, 1073–1079.
89 A. Apblett, F. Grein, J. P. Johnson, J. Passmore and P. S. White, *Inorg. Chem.*, 1986, **25**, 422–426.
90 *SHELXTL 5.03*, Siemens Analytical Instruments, 1994.
91 *CRYSTALCLEAR, 1.4.0 ra 1*, Rigaku Inc., 2008.
92 T. Higashi, *FSPROCESS*, Rigaku Inc., 2001.
93 *SHELXTL 6.14, BRUKER AXS*, 2000.
94 K. Brandenburg, *DIAMOND, 3.1*, Crystal Impact GbR, Bonn, 2009.
95 A. D. Becke, *Phys. Rev. A: At., Mol., Opt. Phys.*, 1988, **38**, 3098.
96 K. Eichkorn, F. Weigend, O. Treutler and R. Ahlrichs, *Theor. Chem. Acc.*, 1997, **97**, 119–124.
97 A. Schaefer, H. Horn and R. Ahlrichs, *J. Chem. Phys.*, 1992, **97**, 2571–2577.
98 J. P. Perdew, *Phys. Rev. B*, 1986, **33**, 8822.
99 J. P. Perdew, K. Burke and M. Ernzerhof, *Phys. Rev. Lett.*, 1996, **77**, 3865–3868.
100 J. P. Perdew, M. Ernzerhof and K. Burke, *J. Chem. Phys.*, 1996, **105**, 9982–9985.
101 F. Weigend and R. Ahlrichs, *Phys. Chem. Chem. Phys.*, 2005, **7**, 3297–3305.
102 D. Andrae, U. Häußermann, M. Dolg, H. Stoll and H. Preuß, *Theor. Chim. Acta*, 1990, **77**, 123–141.
103 R. Ahlrichs, M. Baer, M. Haeser, H. Horn and C. Koelmel, *Chem. Phys. Lett.*, 1989, **162**, 165–169.
104 F. Weigend and M. Häser, *Theor. Chem. Acc.*, 1997, **97**, 331–340.
105 F. Weigend, M. Häser, H. Patzelt and R. Ahlrichs, *Chem. Phys. Lett.*, 1998, **294**, 143–152.
106 Best to our knowledge there are no literature values for the def2-TZVPP basis set in combination with the PBE0 hybrid-functional. Moran *et al.* (*J. Phys. Chem. A*, 2007, **111**, 11683) report scaling factors for ΔH^{298} with the basis 6-311+G(2df,p) and PBE0 of 0.9720.
107 C. Ehrhardt and R. Ahlrichs, *Theor. Chim. Acta*, 1985, **68**, 231–245.
108 R. Heinzmann and R. Ahlrichs, *Theor. Chim. Acta*, 1976, **42**, 33–45.
109 A. Lavalette, G. A. Lawrance, N. W. Alcock and M. J. Hannon, *Eur. J. Inorg. Chem.*, 2004, 3981–3983.

